Correspondence

Homodyne Detection of Phase-Modulated Light*

A technique for detecting a phase-modulated light beam without the use of an optical discriminator has been devised and demonstrated in this laboratory. Homodyne amplification has also been observed and conforms to the theoretical expectation. The demodulation of PM occurs when the carrier and local oscillator beams are in quadrature at the detector.[1,2]

The optical homodyne system used to verify the demodulation is depicted in Fig. 1. The laser beam radiated by source, S, is divided by beamsplitter, B, into two beams. One beam is phase-modulated by a moving mirror driven at an angular frequency, ω_m, by a piezoelectric crystal, and attenuated at A. The second beam is unmodified and plays the role of the local oscillator when the beams are recombined on the photosensitive surface of a square-law detector.

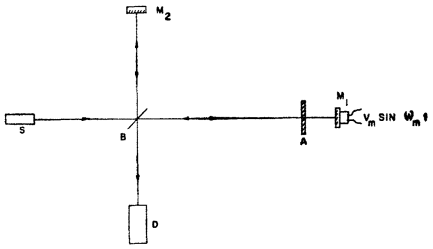

Fig. 1—Experimental arrangement for detection of phase-modulated light by optical homodyne method.
S = laser light source
B = beam splitter
M_1 = velocity-modulated mirror (signal beam)
M_2 = stationary mirror (local oscillator beam)
D = detector
A = attenuator.

The PM demodulation process can be understood with the aid of Fig. 2. In this phasor diagram, the time dependence of amplitude- and frequency-modulated fields is represented, for small modulation depths, by the projection of rotating vectors. The carrier vector rotates at a frequency, ω, and the sideband vectors rotate at frequencies, $\pm\omega_m$, with respect to the carrier. In the case of PM, the resultant of the sideband vectors is always in quadrature with the rotating carrier vector; in the case of AM, the sideband resultant is in phase with the carrier, ($\psi=0$). The polarizations of all the components are presumed the same, as are the field distributions across the beam.

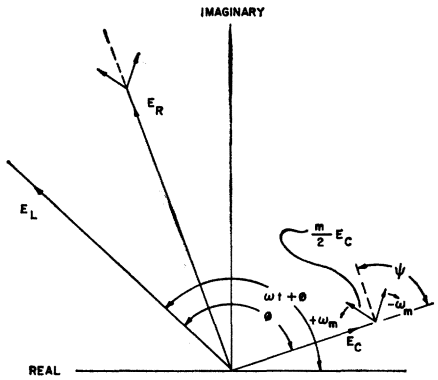

Fig. 2—Phasor diagram showing conversion of PM signal into AM resultant by vector addition with local oscillator.

In a homodyne system the relative phase of the carrier and local oscillator beams at the detector can be varied so that their resultant vector has any desired phase angle with respect to the sideband resultant. When the total resultant and the sideband resultant are in phase, a purely AM wave impinges on the detector. Thus, with proper adjustment of relative optical phase, PM sidebands of the carrier become AM sidebands of the local oscillator beam. Detection of the latter modulation is conventional.

An analytical description of the vector diagram, valid for small m, is given by the following equation for the total field at the detector:

$$\mathcal{E}_R = \mathrm{Re}\left\{E_L e^{i(\omega t+\phi)} + E_C e^{i\omega t} + \frac{mE_C}{2}\left[e^{i(\omega t-\omega_m t+\psi)} + e^{i(\omega t+\omega_m t+\psi)}\right]\right\}. \quad (1)$$

The first term on the right gives the magnitude and phase of the local oscillator field; the second term describes the signal carrier; the last two terms represent sidebands generated by sinusoidal modulation at a frequency, ω_m, with modulation index m. The phase angle of the sidebands with respect to the carrier is ψ.

In a square-law detector the photocurrent is proportional to the mean square of the field,

$$i \propto \overline{\mathcal{E}_R^2}, \qquad \frac{1}{\omega_m} \gg \tau \gg \frac{1}{\omega}. \quad (2)$$

The response time τ of the detector includes many optical cycles, but is small compared to the period of the modulation. For the practical case in which the local oscillator field is much larger than the carrier, the leading terms in the photocurrent reduce to

$$i \propto \overline{\mathcal{E}_R^2} = \frac{E_L^2}{2} + mE_L E_C \cos(\psi-\phi)\cos\omega_m t. \quad (3)$$

The homodyne-amplified signal current is now amplitude modulated and its magnitude is multiplied by the constant factor, $\cos(\psi-\phi)$, which may be made identically zero or, for maximum amplification, equal to unity. When the carrier is phase modulated, $\psi = \pm\pi/2$. Thus the local oscillator phase angle must be adjusted to $\phi = \pm\pi/2$ in order to demodulate a phase-modulated wave. The same technique can be used to demodulate a mixture of AM and PM (ψ arbitrary). Such a mixture may be generated when the signal passes through a dispersive medium.

The dependence of the homodyne amplification on beam intensity was observed, using calibrated attenuators. By measuring intensity ratios it was verified that the homodyne crossterm in the photocurrent varied as $i \propto \sqrt{P_L P_C}$, where P is the beam power.

One limitation of this technique is that, for a large index of modulation, the resulting amplitude modulation is a sinusoidal rather than a linear representation of the phase modulation. However, we are using this same deviation from linearity to generate a suitable error signal for locking two lasers at any desired phase difference, an essential requirement for any optical homodyne communication link.

The authors would like to thank R. T. Daly for many helpful discussions.

P. Rabinowitz
S. Jacobs
R. Targ
G. Gould
TRG Inc.
Syosset, N. Y.

Mode Suppression and Single Frequency Operation in Gaseous Optical Masers*

This communication reports results[1] of mode suppression experiments with gaseous optical masers. We have observed the suppression of unwanted longitudinal modes in an inherently multimode He-Ne maser oscillator. Our experiments were carried out on each of the two transitions of neon: $2s_2$-$2p_4$ at 11,523 Å,[2] and $3s_2$-$2p_4$ at 6328 Å.[3]

* Received September 24, 1962; revised manuscript received, September 26, 1962. The work for this note was accomplished under an optical communications development program partially supported by the Communications Branch of ASD (AF33(657)-8060) and by the Advanced Communications Techniques Branch of RADC (AF30(602)-2591).

[1] This homodyne PM demodulation principle was first applied at RF frequencies by M. G. Crosby, "Communication by phase modulation," PROC. IRE, vol. 27, pp. 126–136; February, 1939.

[2] Recently, another method for detecting phase modulation of light has been proposed: phase modulation of a light beam can be converted into space modulation by an optical dispersing element; space modulation can then generate a transverse electron beam-wave at a photocathode. See S. E. Harris and A. E. Siegman, "A proposed FM phototube for demodulating microwave-frequency-modulated light signals," IRE TRANS. ON ELECTRON DEVICES, vol. ED-9, pp. 322–329; July, 1962.

* Received September 17, 1962; revised manuscript received September 21, 1962.

[1] The first results were announced by C. K. N. Patel and H. Kogelnik at the meeting of the American Physical Society, Seattle, Wash.; August 27–29, 1962. (Post deadline paper.)

[2] A. Javan, W. R. Bennett, Jr., and D. R. Herriott, "Population inversion and continuous optical maser oscillation in a gas discharge containing a He-Ne mixture," *Phys. Rev. Lett.*, vol. 6, pp. 106–110; February, 1961.

[3] A. D. White and J. D. Rigden, "Continuous gas maser operation in the visible," PROC. IRE (*Correspondence*), vol. 50, p. 1697; July, 1962.

Normally the resonators used in conjunction with these masers have consisted of Fabry-Perot cavities formed by a pair of either plane-parallel or concave mirrors.[2-6] For a practical mirror separation of 1 meter, one has a frequency separation of 150 Mc between adjacent longitudinal modes. The Doppler-broadened linewidth of the 11,523 Å transition is about 800 Mc.[7] Thus, under practical operating conditions, the maser will oscillate simultaneously at several optical frequencies. However, for most scientific and technological applications, one desires a single frequency output. This is most simply obtained by using maser cavities of the shortest possible mirror separation, thus sacrificing gain and output power.

Kleinman and Kisliuk[8] have described theoretically the behavior of a four-reflector plane-parallel mirror arrangement which discriminates against unwanted longitudinal modes of a Fabry-Perot resonator.[9] We describe here an arrangement consisting of three concave mirrors, for suppressing the unwanted modes. Both arrangements are based on interference effects and do not require the reduction in the length of the amplifying medium. As shown in Fig. 1, our scheme consists in adding to the "primary" maser cavity (formed by mirrors A and B) a "secondary" cavity (formed by mirrors B and C). The radii of curvature of all the reflecting surfaces are equal, and mirrors A and C are spaced to be confocal. Now all mirror surfaces fit surfaces of constant phase of a confocal mode,[5] regardless of the spacing between A and B. The field distribution between the three mirrors is the same as that of a longitudinally asymmetric mode[10] of the confocal resonator formed by mirrors A and C. Mirror B may be replaced by a flat mirror or by a mirror of any arbitrary curvature, as long as the primary cavity AB is stable.[9] In addition to offering ease of adjustment our schemes allow one to optimize the transmittance of mirror A for maximum power output.

Due to the interference effects the effective reflection coefficient looking into the secondary cavity varies periodically with frequency,[11] the period being determined by the spacing BC. The positions of the maxima and minima of the reflectivity depend critically on this spacing. As the reflection coefficient of the secondary cavity is in general complex valued, the resonance frequencies of the primary cavity are perturbed, but if the reflection coefficient of C is smaller than that of B, this effect is small. The gain of the He-Ne maser medium is relatively low (about 10 per cent per meter). Hence, reducing the reflection coefficient at a particular frequency by a relatively small amount is sufficient to prevent oscillation at that frequency.

We used gas discharge tubes with Brewster angle windows and external concave mirrors.[6] We employed the arrangement shown in Fig. 1 with three mirrors having a radius of curvature of 2 meters. The reflectivity of A and B was about 99 per cent. Mirror B had an antireflection coating on the second surface to prevent additional interference. The reflectivity of C was typically between 80 and 90 per cent. These values, however, do not represent optimum values which have yet to be determined.

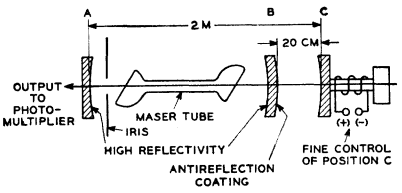

Fig. 1.

The maser output was taken through mirror A and was detected with a suitable photomultiplier. The beat frequencies[2,7] between the various longitudinal modes oscillating were observed on a spectrum analyzer. An iris of about 3- to 5-mm diameter was inserted within the primary cavity to prevent oscillation on all but the fundamental transverse mode.

The 20-cm separation between mirrors B and C was controlled within a fraction of a wavelength, using either a differential thread system or a magnetostrictive device.[7,12] For this spacing the frequency difference between consecutive minima of the reflection coefficient of the secondary cavity is 750 Mc. Mode suppression results obtained were:

1) With mirror C blocked the output power of the oscillating maser was measured, and the amplitudes of the beat frequencies at 80, 160, 240, 320, etc, Mc were noted. The presence of the beats indicates a multifrequency output.
2) With mirror C unblocked the amplitudes of all the measurable beats were reduced, due to interference effects, by at least a factor of 10, and the higher beats beyond 320 Mc could no longer be detected. The output power increased by about 50 per cent.

We have now obtained essentially a single-frequency output. The maser is oscillating in a single mode close to the center of the Doppler-broadened gain curve. The other modes falling within the gain curve no longer oscillate because of increased loss at these frequencies. The increase of power output is mainly the result of increased reflectivity of the secondary cavity at the oscillating frequency.

H. KOGELNIK
C. K. N. PATEL
Bell Telephone Labs., Inc.
Murray Hill, N. J.

Simultaneous Gas Maser Action in the Visible and Infrared*

A nearly confocal helium-neon maser with external mirrors[1] has been made to oscillate simultaneously at 6328Å and at four wavelengths in the infrared, 11,526Å, 11,617Å, 11,770Å and 11,988Å. The visible oscillation has been reported by White and Rigden[2] and three of the infrared lines have been reported by Javan, Bennett and Herriott.[3] The fourth line at 11,770Å ($2s_2 \rightarrow 2p_2$) has been seen by McFarlane, *et al.*[4]

The maser tube was 1 meter long, 6 mm in diameter and was excited by a dc discharge. The voltage drop across the discharge was approximately 1700 v and currents between 10 and 100 ma were used. A 10:1 mixture[5] of He-Ne filled the maser tube at a total pressure of 0.7 mm of Hg. The mirrors were 90 cm in radius and were spaced approximately 150 cm apart. The dielectric coatings on the doubly peaked or "hybrid" mirrors were designed to give maxima of reflection, both at 11,500Å and at 6330Å. Specifically, eleven layers were laid down first for peak reflection in the infrared; then, after a transition layer, a nine-layer system was deposited for peak reflection at 6330Å. The power measurements were made using a calibrated Eppley thermopile and a high-speed Perkin-Elmer thermopile attached to a spectrometer. Relative power measurements of the infrared lines were made with the spectrometer and the absolute powers in the visible and the total of the four infrared lines were meas-

* Received September 26, 1962.

[1] W. W. Rigrod, H. Kogelnik, D. Brangaccio, and D. R. Herriott, "Gaseous optical maser with external concave mirrors," *J. Appl. Phys.*, vol. 33, pp. 743–744; February, 1962.

[2] A. D. White and J. D. Rigden, "Continuous gas-maser operation in the visible," PROC. IRE (*Correspondence*), vol. 50, p. 1697; July, 1962.

[3] A. Javan, W. R. Bennett, Jr., and D. R. Herriott, "Population inversion and continuous maser oscillation in a gas discharge containing a He-Ne mixture," *Phys. Rev. Lett.*, vol. 6, p. 106; February, 1961.

[4] R. A. McFarlane, C. K. N. Patel, W. R. Bennett, Jr., and W. L. Faust, "New Helium-Neon Optical Maser Transitions," PROC. IRE (*Correspondence*), vol. 50, pp. 2111–2112; October, 1962.

[5] The optimum mixture for maser action in the visible is found to be a 5:1 mixture of He-Ne at a total pressure of 0.6 mm of Hg. This confirms a measurement of C. K. N. Patel (private communication).

[4] A. G. Fox and T. Li, "Resonant modes in a maser interferometer," *Bell Sys. Tech. J.*, vol. 40, pp. 453–488; March, 1961.

[5] G. D. Boyd and J. P. Gordon, "Confocal multimode resonator for millimeter through optical wavelength masers," *Bell Sys. Tech. J.*, vol. 40, pp. 489–508; March, 1961.

[6] W. W. Rigrod, H. Kogelnik, D. J. Brangaccio, and D. R. Herriott, "Gaseous optical maser with external concave mirrors," *J. Appl. Phys.*, vol. 33, pp. 743–744; February, 1962).

[7] W. R. Bennett, Jr., "Hole burning effects in a He-Ne optical maser," *Phys. Rev.*, vol. 126, pp. 580–593; April, 1962.

[8] D. A. Kleinman and P. P. Kisliuk, "Discrimination against unwanted orders in the Fabry-Perot resonator," *Bell Sys. Tech. J.*, vol. 41, pp. 453–462; March, 1962.

[9] A scheme using three plane mirrors has been considered recently by T. R. Koehler and J. P. Goldsborough, "Three-reflector optical cavity for mode discrimination," *Bull. Am. Phys. Soc.*, vol. 7, p. 446; August, 1962.

[10] G. D. Boyd and H. Kogelnik, "Generalized confocal resonator theory," *Bell Sys. Tech. J.*, vol. 41, pp. 1347–1369; July, 1962.

[11] M. Born and E. Wolf, "Principles of Optics," Pergamon Press, New York, N. Y., p. 326; 1959.

[12] M. Pascalau, E. Weissman, and E. Tataru, "Fabry-Perot interferometer with magnetostrictive analyzing," *Acad. Rep. Pop. Romine, Inst. Fiz. Studii Cercetari Fiz.*, vol. 12, pp. 843–852; April, 1961.

ured with the Eppley thermopile and selective filters.

A diagram of the energy levels involved in the five maser transitions is shown in Fig. 1. Stable maser action was observed at 6328Å ($3s_2 \rightarrow 2p_4$), 11,526Å ($2s_2 \rightarrow 2p_4$); 11,617Å ($2s_3 \rightarrow 2p_5$); 11,770Å ($2s_2 \rightarrow 2p_2$) and at 11,988Å ($2s_3 \rightarrow 2p_2$). The power output for the visible and strongest infrared lines as a function of tube current using the hybrid mirrors is shown in Fig. 2. The absolute power output with infrared mirrors had a maximum value of approximately 4 mw total in the same four lines.

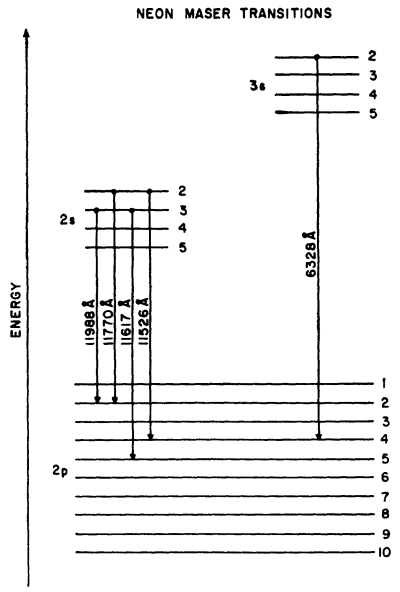

Fig. 1.

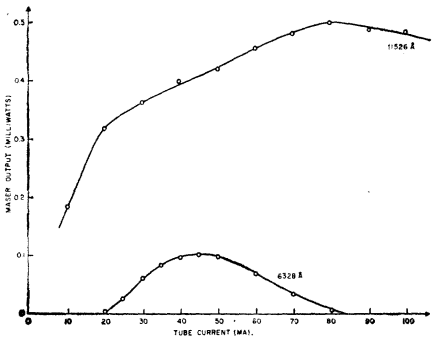

Fig. 2.

It can be seen from Fig. 1 that the 6328Å and 11,526Å maser lines have the same terminal level. It is to be expected that simultaneous oscillation at these two wavelengths will decrease the power output of both of them from the values obtained when the maser oscillates at only one of the wavelengths. This is confirmed for the 11,526Å line by the results shown in Fig. 2. For currents up to 20 ma only the infrared line is oscillating. At higher currents the maser oscillates at 6328Å and apparently decreases the gain at 11,526Å by increasing the population of their common lower level. At currents greater than 50 ma the visible output gradually decreases and finally vanishes while the infrared line maintains a relatively constant output up to 100 ma. It is interesting to note that the sum of the (absolute) power curves for these two transitions forms a smooth curve of the same general shape as the curve for the infrared line alone when infrared mirrors are used. It remains to be seen whether this is merely fortuitous or whether the 6328Å output actually equals the drop in power observed in the 11,526Å line.

The 11,770Å and 11,988Å lines also terminate on a common level ($2p_2$) and both peak at an intensity of about 0.1 mw. However, it was not possible to get one of them to oscillate selectively over the full current range and power coupling could not be observed. The 11,617Å line had a peak intensity of 0.15 mw.

The simultaneous maser oscillations obtained using hybrid mirrors were stable and showed no relaxation oscillations slower than 10^7 cps, which was the bandwidth of the detector used to observe the output.

J. D. Rigden
A. D. White
Bell Telephone Labs., Inc.
Murray Hill, N. J.

Ruby Laser Operation in the Near IR*

In the course of experiments with a pulsed reflector laser of the type described by Hellwarth and McClug[1,2] we have observed a stimulated emission at approximately 7670 Å accompanying the usual 6943 Å emission. For the particular laser used, the energy at 7670 Å is about one fifth that at 6943 Å. The collimination of the beam appears to be about six milliradians at both wavelengths. The wavelength 7670 Å does not coincide with the wavelength of any lines which have been reported[3] in the fluorescent spectrum of ruby.

The experimental arrangement uses a $\frac{1}{4} \times 3$ inch ruby, polished on all surfaces, which had a 90°C axis with respect to the cylinder axis. The Fabry-Perot interferometer was formed by external dielectric flats with 99.8 per cent reflectivity and 50 per cent reflectivity, respectively. The reflectivity varied only slightly over the wavelength region of interest. The optical switching was provided by a nitrobenzene-filled Kerr cell and a Wollaston prism. The lamp energy was supplied from a transmission line and the resulting light pulse had a nearly square shape in time with a duration of about 350 μsec. The Kerr cell was adjusted to open 400 μsec after the initiation of the light pulse. The 6943 Å radiation was isolated by using an interference filter of 50 Å half width. The 7670 Å radiation was separated by means of Wratten 88A low-pass filter. Metallic film neutral density filters were used for attenuation where needed. A 925 phototube with an S-1 cathode was used as a detector for most of the measurements, although a type 6217 photomultiplier with an S-10 cathode was used in some of the initial measurements. This latter tube was discarded because the sensitivity of the S-10 cathode is a strong function of wavelength. Using the same filters, the absolute energy at each wavelength was measured with a calorimeter of the type described by Li and Sims.[4] These measurements were made at a driving energy of 575 joules into the flashtube and showed an output of about 200 millijoules at 6943 Å and 30 to 40 millijoules at 7670 Å.

The wavelength was obtained using a modified Bechman DU spectrophotometer as a monochromator. This limits the wavelength accuracy to about ±15 Å.

When the Kerr cell is disabled, the laser operates in the "classical" fashion. In this mode of operation we have not observed any 7670 Å radiation although our equipment is such that a fraction of a millijoule should be detectable.

Our observations of the pulse shape indicate that the width of the pulse at both wavelengths is 16–20 nsec (the resolving time of our equipment). In the case of the 6943 Å emission two or three such pulses with spacings of 20 nsec are common. Successive pulses have rapidly decreasing amplitudes. At 7670 Å the secondary pulses are much smaller; in fact more than a minute second pulse has never been observed.

E. J. Woodbury
W. K. Ng
Hughes Aircraft Co.
Culver City, Calif.

[4] T. Li and S. D. Sims, "A calorimeter for energy measurements of optical masers," *Appl. Optics*, vol. 1, pp. 325–328; May, 1962.

The Granularity of Scattered Optical Maser Light*

When the continuous gas maser was first operated at 6328 Å[1] and the beam projected onto the laboratory wall, it was obvious to all present that there was something very unusual about the scattered maser

* Received July 25, 1962. This work was supported in part by the U. S. Army Signal Corps under Contract No. DA36-039-SC88936 for ARPA Project Defender.

[1] R. W. Hellwarth, "Control of Fuorescent Pulsations," in "Advances in Quantum Electronics," Columbia University Press, New York, N. Y., p. 334; 1961.

[2] F. J. McClung and R. W. Hellwarth, "Giant optical pulsations from ruby," *J. Appl. Phys.*, vol. 33, pp. 828–829; March, 1962.

[3] P. Pringsheim, "Fuorescence and Phosphorescence," Interscience Publishers Inc., New York, N. Y., pp. 637–646; 1949.

* Received September 13, 1962.

[1] A. D. White and J. D. Rigden, "Continuous gas maser operation in the visible," Proc. IRE (*Correspondence*), vol. 50, p. 1697; July, 1962.

light. The bright area of red light showed a remarkable granular or peppery nature not present in ordinary light. The granularity also appeared to scintillate since the granular pattern moved when there was relative motion between the surface and the observer.

Although the phenomenon is present in the scattered light from other masers, it had not been observed earlier for rather obvious reasons. The granularity is not intrinsic to the maser since it does not appear in direct images of the beam, but rather in the scattered light; it is not in the eye since it occurs in all image-forming devices. When the surface is moved rapidly or randomly, the granularity disappears. For example, it is not seen in the scattered light from a rotating wheel or from colloidal suspensions such as milk. A slowly rotating wheel or frozen milk show the granularity.

One of the most obvious features of the granularity is that its apparent size or coarseness is a function of the angular aperture or f number of the optical system, the size increasing with decreasing apertures. The series of photographs shown in Fig. 1 was taken with successively smaller apertures. The variations in coarseness are most dramatically observed by interposing a variable iris in front of the eye.

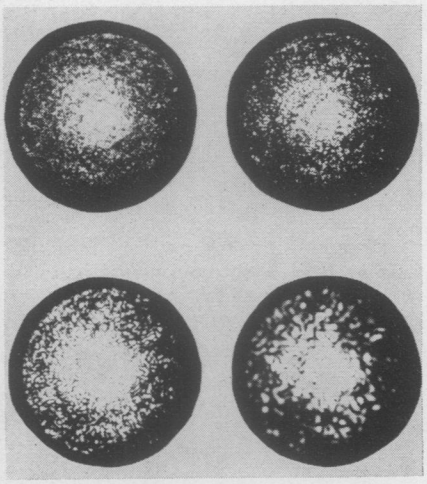

Fig. 1—Photographs of a scattering surface taken with increasing f number.

In order to understand the precise nature of the interference phenomenon responsible for the granularity, we performed a number of experiments with a limiting iris in an optical system so that the detail of the granularity could be viewed under high magnification. The character of the granularity is a function of the shape of the limiting aperture. For circular apertures, the granularity consists of a random juxtaposition of irregularly shaped bright areas on a darker background; while for narrow slits, the granularity consists of roughly parallel lines running perpendicular to the slit. The granularity is not a function of intensity.

The general appearance of the granularity is essentially independent of the character of the scattering surface. For example, we made surfaces by densely packing particles of known size from 0.1-μ alumina powder to coarse carborundum grit. By grading the packing density of small particles on a glass slide which was illuminated by the maser beam, we could see the diffraction pattern, associated with the limiting aperture, in the scattered light from individual particles. Occasionally, individual particles would be close enough so that the diffraction patterns could partially overlap, forming a dark intersection line which distorted the shape of the central bright disk. As the particle density increased further, the characteristic granularity appeared.

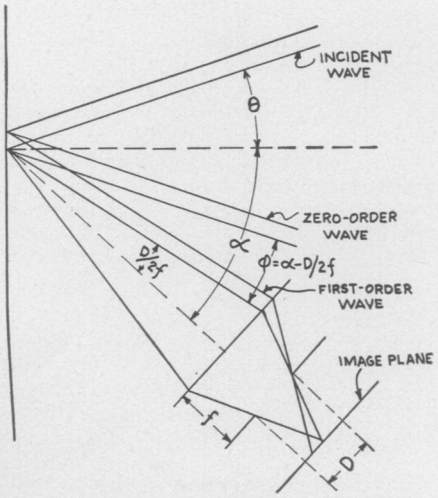

Fig. 2—Schematic of image-forming system showing the band-pass properties of a lens aperture.

Thus, an intuitive explanation of the granularity could be given as follows. The granularity arises from the interference of completely coherent diffraction patterns. The size and shape of the diffraction patterns are determined by the aperture of the viewing system. The centers of the diffraction patterns are positioned at randomly located points which scatter strongly in the direction of the observer. The motion of the granularity and the "washout" when the scattering surface is moved is therefore easily explained.

The motion of the granularity when the observer moves can be understood by noting that the plane of focus of the observer seldom corresponds to the scattering surface. The motion is a result of parallax. The relative direction of motion reverses as the plane of focus is moved from behind to in front of the scattering plane.

An analytical description of the granularity can be given and the equivalent physical description will be sketched briefly. As a result of this analysis, we became convinced that the granularity could be observed with nonmaser light when the illuminating beam was to some extent diffraction limited. We have since observed the granularity in unfiltered sunlight and in the light of a high-pressure mercury arc.

Consider Fig. 2 which shows a parallel beam of light of wavelength λ incident on a one-dimensional scattering surface at an angle θ. The observer views the scattered light at some angle α usually different from θ. The scattering surface produces a wavefront, associated with the scattered light, with randomly varying amplitude and phase. If we consider a particular Fourier component of the wavefront with periodicity L, which is equivalent to the light scattered from a sinusoidal grating, then the scattered light associated with this component consists of a zero-order parallel beam moving at the angle θ and two first-order parallel beams making angles $\phi \approx \lambda/L\cos\theta$ with respect to the zero-order beam. These beams are focused in the focal plane of the lens, a distance f beyond the lens.

The aperture of the optical system of width D is assumed to be in the focal plane of the lens. If $\alpha - D/2f < \phi + \theta < \alpha + D/2f$, the first order beam will be passed by the optical system. The image will only contain spatial beats between those particular Fourier components of the scattering surface with periodicity $2\pi(\alpha - \theta - D/2f)\cos\theta/\lambda < 2\pi/L < (\alpha - \theta + D/2f)\cos\theta/\lambda$. Thus, the optical system acts as a band-pass filter. A noise input arises from the random Fourier components of the scattering surface. It is well known that the detected output of a band-limiting filter fed by noise appears to contain beats at a frequency approximating the band pass. Thus, the variations or beats in the image appear to have approximately a periodic spacing $f\lambda/D$. This variation is the observed granularity. The extension to two dimensions is obvious.

From this description it is clear that a range of wavelengths in the incident beam will not destroy the granularity. On the other hand, a range of incident angles could easily wash out the granularity because of the averaging produced by the superposition of the associated, incoherent, randomly positioned, beat patterns. Thus, the significant feature of the maser light in producing this phenomenon is not the spectral purity, but rather the fact that the angular spread of the beam is diffraction limited.

J. D. Rigden
E. I. Gordon
Bell Telephone Labs., Inc.
Murray Hill, N. J.

WWV and WWVH Standard Frequency and Time Transmissions*

The frequencies of the National Bureau of Standards radio stations WWV and WWVH are kept in agreement with respect to each other and have been maintained as constant as possible since December 1, 1957,

* Received September 21, 1962.

with respect to an improved United States Frequency Standard (USFS).[1] The corrections reported here were arrived at by means of improved measurement methods based on transmissions from the NBS stations WWVB (60 kc) and WWVL (20 kc). The values given in the table are 5-day running averages of the daily 24-hour values for the period beginning at 1800 UT of each day listed.

The time signals of WWV and WWVH are also kept in agreement with each other. Since these signals are locked to the frequency of the transmissions, a continuous departure form UT2 may occur. Corrections are determined and published by the U. S. Naval Observatory. The time signals are maintained in close agreement with UT2 by properly offsetting the broadcast frequency from the USFS at the beginning of each year when necessary. This new system was commenced on January 1, 1960.

WWV Frequency
With Respect to U. S. Frequency Standard

1962		Parts in 10^{10}*
August	1	−130.1
	2	−130.1
	3	−130.1
	4	−130.1
	5	−130.2
	6	−130.2
	7	−130.2
	8	−130.2
	9	−130.2
	10	−130.1
	11	−130.0
	12	−129.9
	13	−129.8
	14	−129.7
	15	−129.7
	16	−129.6
	17	−129.5
	18	−130.3†
	19	−130.2
	20	−130.1
	21	−130.1
	22	−130.0
	23	−130.0
	24	−130.0
	25	−129.9
	26	−129.8
	27	−129.7
	28	−129.7
	29	−129.7
	30	−129.6
	31	−129.7
	Monthly mean:	−129.9

* A minus sign indicates that the broadcast frequency was below nominal. The uncertainty associated with these values is $\pm 5 \times 10^{-11}$.
† WWV frequency adjusted as follows:
August 18, -1.0×10^{-10} Adjustment, 1900 UT.

Subsequent changes were as follows:

Frequency Offset, with Reference to the USFS
January 1, 1960, −150 parts in 10^{10}
January 1, 1962, −130 parts in 10^{10}

Time Adjustments, with Reference to the Time Scale UT2

December 16, 1959, retardation, 20 milliseconds
January 1, 1961, retardation, 5 milliseconds
August 1, 1961, advancement, 50 milliseconds.

Adjustments were made at 0000 UT on the foregoing dates: an advancement means that the signals were adjusted to occur at an earlier time than before.

National Bureau of Standards
Boulder, Colo.

[1] See "National standards of time and frequency in the United States," Proc. IRE (*Correspondence*), vol. 48, pp. 105–106; January, 1960.

Detection and Amplification of the Microwave Signal in Laser Light by a Parametric Diode*

McMurtry and Siegman[1] have reported the detection and amplification of microwave signals in laser light by a conventional traveling-wave tube with an oxide-coated cathode. Since this utilizes the square-law characteristic of the "external photoelectric effect" of the photocathode, we may also expect a similar result from the "internal photoelectric effect." With the latter effect, the frequency range of the light for detection may be easily extended to near-infrared region, by using narrow energy band gap materials.

We have tested a semiconductor point-contact diode to check the possibility of detection of the microwave signal in laser light, and obtained an interesting result. The diode is a Nippon Electric's type GSB-1, silver-bonded germanium, glass-sealed, parametric diode. The diode is placed in a parametric amplifier as shown in Fig. 1, and illuminated by ruby laser light through a hole on the cavity-wall. The ruby laser, Raytheon's model LH-1, is pumped at the level of 288 joules. The ruby crystal is 0.05 per cent chromium ion doped, and the rod dimensions are 2.5 inches as long and 0.25 inches in diameter. The laser light is reflected by a half-mirror (96 per cent reflectance) and thrown through the hole to the diode without collimation or focusing. Behind the mirror, a phototube is placed as a light monitor.

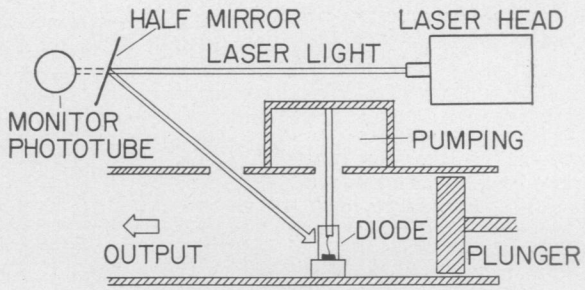

Fig. 1—Schematic diagram of parametric amplifier.

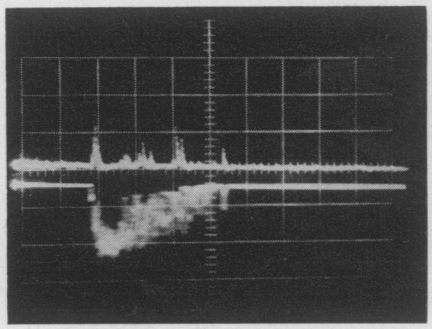

Fig. 2—Output of laser detection. Upper trace is the receiver output at 3957 Mc. No parametric pumping power is supplied. Lower trace is the monitoring phototube output. The time scale is 100 μsec/div.

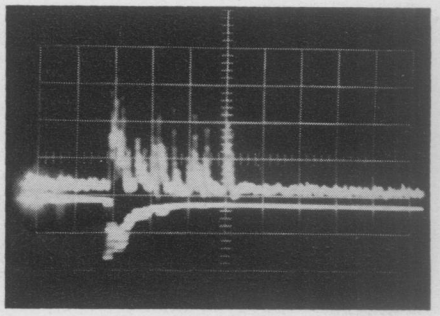

Fig. 3—Output of laser detection. Upper trace is the receiver output at 3957 Mc, in the same scale as in Fig. 2, when the pumping power (7914 Mc) is supplied, and the amplifier gain is 15 db. Lower trace is the diode current, 40 μA/div. The time scale is 100 μsec/div.

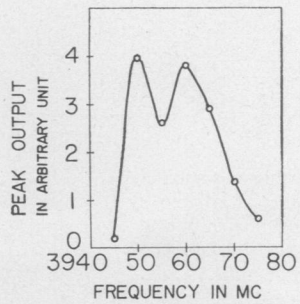

Fig. 4—Output spectrum of the third beat component of the ruby laser light.

* Received August 27, 1962.

[1] B. J. McMurtry and A. E. Siegman, "Photomixing experiments with a ruby optical maser and a traveling-wave microwave phototube," *Appl. Optics*, vol. 1, pp. 51–53; January, 1962.

The output of the parametric amplifier is fed to a conventional 4-kMc receiver through an isolator (there is no need of circulator). The third beat component of the multimode laser output is detected. This frequency is calculated to be 4026 Mc, but the observed value is 3957 Mc. Upper traces of Figs. 2 and 3 show the receiver video outputs, without and with the parametric pumping power, respectively. The vertical scales are identical for both.

When no parametric pumping power is applied, only short and sparse impulses are observed as shown in Fig. 2. When the pumping power is supplied, and the gain as an ordinary amplifier is approximately 15 db, they are amplified as in Fig. 3. Lower traces of Figs. 2 and 3, are the output of the monitoring phototube and the backward diode current, respectively. Fig. 4 shows the output spectrum. The equivalent input power of beat component is approximately —70 dBm at the maximum. The gain of the parametric amplifier changes during the laser light illumination. The change depends on the plunger position (Fig. 1). When the plunger is moved toward the diode from a neutral point, the gain increases during the illumination, and when it is moved away from the diode, the gain decreases. From this we may conclude that some increase of junction capacitance is taking place during the illumination.

S. Saito
K. Kurokawa
Y. Fujii
T. Kimura
Y. Uno
The Institute of Industrial Science
University of Tokyo
Tokyo, Japan

Poynting Vector in Linear M-Type Tubes*

As an extension of the previous work,[1] this note presents applications of a few vector identities for a Poynting power flow inside a thick electron beam in the interaction region of a linear M-type tube.

The linear M-type tube under consideration has a geometry independent of x, and electrons and EM waves travel along the z axis as shown in the previous note.[1] Although RF signals can assume any time dependence besides harmonic variations, all field quantities must be single-valued, excluding crossovers of electron paths. This note does not resort to Riemann geometry. The use of volume charge density, ρ and the z component of Poynting vector, S_z excludes singular types of sheet beams and pencil beams.

Substitute ∇, $\bar{E}$, $\bar{E}$ and $\bar{H}$, respectively, for $\bar{a}$, $\bar{b}$, $\bar{c}$, and $\bar{d}$ in the vector identity below,[2]

$$(\bar{a}\times\bar{b})\times(\bar{c}\times\bar{d}) = (\bar{a}\times\bar{b}\cdot\bar{d})\bar{c} - (\bar{a}\times\bar{b}\cdot\bar{c})\bar{d}, \quad (1)$$

so that

$$\frac{1}{2}\frac{\partial\bar{H}^2}{\partial t}\bar{E} = \frac{\partial\bar{H}}{\partial t}\times\bar{S} + \left(\frac{\partial\bar{H}}{\partial t}\cdot\bar{E}\right)\bar{H}, \quad (2)$$

where the Poynting vector $\bar{S}$ stands for $\bar{E}\times\bar{H}$.

A similar expression for $\bar{H}$ is derived from the set of ∇, $\bar{H}$, $\bar{E}$ and $\bar{H}$. In doing so the terms $\bar{J}\times\bar{S}$ appearing on both sides of (1) are automatically cancelled for the current-present cases of Maxwell's equations.

Now substitute ∇, $\bar{H}$, $\bar{E}$ and $\bar{H}$, respectively, for $\bar{a}$, $\bar{b}$, $\bar{c}$ and $\bar{d}$ in the formula below,

$$(\bar{a}\times\bar{b})\cdot(\bar{c}\times\bar{d}) = \begin{vmatrix} \bar{a}\cdot\bar{c} & \bar{b}\cdot\bar{c} \\ \bar{a}\cdot\bar{d} & \bar{b}\cdot\bar{d} \end{vmatrix}. \quad (3)$$

The result is simplified as

$$(\bar{H}^2 - \epsilon_0\bar{u}\cdot\bar{S})\rho = \epsilon_0\frac{\partial\bar{D}}{\partial t}\cdot\bar{S}, \quad (4)$$

where $\bar{J}$, the convection current density inside the electron beam is represented by $\rho\bar{u}$, and $\bar{u}$ is a two dimensional electron velocity vector.

Electron dynamics in crossed fields entails Lorentz' force equation,

$$m\frac{d\bar{u}}{dt} = -e[\bar{E} + \bar{u}\times\bar{B}_0], \quad (5)$$

where the self-magnetic field of electrons are neglected and $\bar{B}_0$ in an externally applied dc magnetic flux along the x axis. $\bar{B}_0$ is used to maintain a proper electron beam profile. Replace $\bar{E}$ in (5) by $\bar{E}$ arising from (2), such that

$$\frac{m}{2}\frac{\partial\bar{H}^2}{\partial t}\frac{d\bar{u}}{dt} = -e\left[\frac{\partial\bar{H}}{\partial t}\times\bar{S} + \left(\frac{\partial\bar{H}}{\partial t}\cdot\bar{E}\right)\bar{H} + \frac{\mu}{2}\frac{\partial\bar{H}^2}{\partial t}\bar{u}\times\bar{H}_0\right]. \quad (6)$$

Next, premultiply both sides of (6) by $\partial\bar{D}/\partial t$ as a vector product. The purpose of this cross product is to create

$$\left(\frac{\partial\bar{D}}{\partial t}\cdot\bar{S}\right)\frac{\partial\bar{H}}{\partial t}$$

from

$$\frac{\partial\bar{D}}{\partial t}\times\left(\frac{\partial\bar{H}}{\partial t}\times\bar{S}\right).$$

However, $(\partial\bar{D}/\partial t\cdot\bar{S})$ appears in (4). Thus a theoretical model of a linear M-type tube has incorporated four Maxwell's equations and Lorentz' force equation at this stage. Field theories of wave-electron interactions are based on physical facts expressed by these equations. The outcome of the above premultiplication of $\partial\bar{D}/\partial t$ is

$$\rho(\bar{u}\cdot\bar{S})\frac{\partial\bar{H}}{\partial t} + \left(\frac{\partial\bar{D}}{\partial t}\cdot\frac{\partial\bar{H}}{\partial t}\right)\bar{S} = \bar{C}, \quad (7)$$

where a shorthand notation $\bar{C}$ designates

$$\bar{C} = \frac{\rho}{\epsilon_0}\bar{H}^2\frac{\partial\bar{H}}{\partial t} + \frac{\partial\bar{D}}{\partial t} \times\left[\frac{m}{2e}\frac{\partial\bar{H}^2}{\partial t}\frac{d\bar{u}}{dt} + \left(\frac{\partial\bar{H}}{\partial t}\cdot\bar{E}\right)\bar{H} + \frac{\mu}{2}\frac{\partial\bar{H}^2}{\partial t}(\bar{u}\times\bar{H}_0)\right].$$

Slow wave structures employed by most of linear M-type tubes guide EM waves and electron beams along the z axis, therefore the Poynting vector inside the electron beam has no x component. In terms of a two-by-two matrix, (7) is rewritten as

$$\begin{vmatrix} \frac{\partial\bar{D}}{\partial t}\cdot\frac{\partial\bar{H}}{\partial t} + w\rho\frac{\partial H_y}{\partial t} & v\rho\frac{\partial H_y}{\partial t} \\ w\rho\frac{\partial H_z}{\partial t} & \frac{\partial\bar{D}}{\partial t}\cdot\frac{\partial\bar{H}}{\partial t} + v\rho\frac{\partial\bar{H}_z}{\partial t} \end{vmatrix} \cdot\begin{pmatrix} S_y \\ S_z \end{pmatrix} = \begin{pmatrix} C_y \\ C_z \end{pmatrix}. \quad (8)$$

Two special cases which do not provide the inverse matrix of (8) are

$$(\nabla\times\bar{E})\cdot\frac{\partial\bar{E}}{\partial t} = 0 \quad \text{and} \quad (\nabla\times\bar{H})\cdot\frac{\partial\bar{H}}{\partial t} = 0.$$

Except for these rare cases, (8) is reformulated as

$$\begin{pmatrix} S_y \\ S_z \end{pmatrix} = \frac{1}{\Delta}\begin{vmatrix} \frac{\partial\bar{D}}{\partial t}\cdot\frac{\partial\bar{H}}{\partial t} + v\rho\frac{\partial H_z}{\partial t} & -v\rho\frac{\partial H_y}{\partial t} \\ -w\rho\frac{\partial H_z}{\partial t} & \frac{\partial\bar{D}}{\partial t}\cdot\frac{\partial\bar{H}}{\partial t} + w\rho\frac{\partial H_y}{\partial t} \end{vmatrix}\begin{pmatrix} C_y \\ C_z \end{pmatrix}, \quad (9)$$

where

$$\Delta = \left(\frac{\partial\bar{D}}{\partial t}\cdot\frac{\partial\bar{H}}{\partial t}\right)\left[\left(\frac{\partial\bar{D}}{\partial t}\cdot\frac{\partial\bar{H}}{\partial t}\right) + \rho\left(\bar{u}\cdot\frac{\partial\bar{H}}{\partial t}\right)\right].$$

As the Poynting vector, $\bar{S}$ has no x component, $\bar{E}$, $\bar{H}$, $\bar{u}$ and ρ which satisfied (9) also must satisfy

$$\bar{x}_0\cdot(\bar{E}\times\bar{H}) = 0 \quad (10)$$

where $\bar{x}_0$ is a unit vector along the x axis.

* Received February 14, 1962; revised manuscript received, April 19, 1962.

[1] I. Sugai, "Vectors for waves and electrons," Proc. IRE (*Correspondence*), vol. 49, pp. 628–629; March, 1961.

[2] J. A. Stratton, "Electromagnetic Theory," McGraw-Hill Book Co., Inc., New York, N. Y., p. 604; 1941.

The ratio of two components of $\overline{S}$, S_y/S_z is an interesting parameter to consider, as it describes physical mechanism of power flow inside the beam. The ratio is

$$\frac{S_y}{S_z}=\frac{\left[J_z\frac{\partial H_z}{\partial t}+\left(\frac{\partial \overline{D}}{\partial t}\cdot\frac{\partial \overline{H}}{\partial t}\right)\right]C_y-J_z\frac{\partial H_y}{\partial t}C_z}{-J_y\frac{\partial H_z}{\partial t}C_y+\left[J_y\frac{\partial H_y}{\partial t}+\left(\frac{\partial \overline{D}}{\partial t}\cdot\frac{\partial \overline{H}}{\partial t}\right)\right]C_z}\cdot \tag{11}$$

Within the frameworks of assumptions, derivations have been exact up to this point. Because (11) is too complicated for analytical solutions, a useful approximation based on physical facts is invoked. The dimension of $\overline{C}$ in mks units is (force) · (current density/time)^2. This indicates that $\overline{C}$ is closely related to force and current density. If electron beams make small ripples, $C_y \ll C_z$ can be assumed reasonably, so that (11) is reduced to

$$\frac{S_y}{S_z}\cong\frac{-J_z\frac{\partial H_y}{\partial t}}{(\nabla\times\overline{H})\cdot\frac{\partial \overline{H}}{\partial t}-J_z\frac{\partial H_z}{\partial t}}\cdot \tag{12}$$

The sign of S_y/S_z indicates that as S_z is positive, S_y is directed to the sole if S_y/S_z is negative, while S_y is directed to anode if S_y/S_z is positive. Because J_z is a nonzero quantity, S_y/S_z depends on time and space variations of the magnetic field. It is desired to make S_y/S_z as small as possible to have a high efficiency tube. To realize this,

1) increase variations of $\overline{H}$ with respect to position,
2) increase variation of H_z with respect to time,
3) decrease variation of H_y with respect to time.

On the other hand, an exact equation to make $S_y=0$ is

$$\frac{C_y}{C_z}=\frac{J_z\frac{\partial H_y}{\partial t}}{J_z\frac{\partial H_z}{\partial t}+\frac{\partial D}{\partial t}\cdot\frac{\partial H}{\partial t}}\cdot \tag{13}$$

A straightforward solution of (13) is not recommended as C_y and C_z contain expressions of ρ and components of $\overline{E}$, $\overline{H}$ and $\bar{u}$.

In conclusion, this communication has shown that simple vectorial operations of field quantities provide a clear physical insight into complicated two-dimensional EM wave-electron beam interactions of a linear M-type tube. These simple derivations should be analyzed before field analyses of M-type tubes are programmed for digital or analog computers.

The writer gratefully acknowledges kind and constructive suggestions made by an internal reviewer of this journal.

IWAO SUGAI
ITT Federal Labs.
Nutley, N. J.

Metric Coefficients for Vector Wave Equations*

This communication considers certain peculiarities connected with the metric coefficients l, m, n of orthogonal curvilinear coordinate systems u, v, w in which the vector wave equation is to be solved.

A few books[1,2] published in the past distinguish div grad ($=\nabla^2$) from grad div-curl curl ($=\text{✡}$). The recent book by Moon and Spencer[3] places considerable emphasis on this difference, using a different operator symbol, ✡, in place of the familiar Laplacian operator, ∇^2. Moon and Spencer express vector and scalar wave equations respectively by

$$\text{✡}\,\overline{F}-\mu\epsilon\frac{\partial^2\overline{F}}{\partial t^2}=0, \tag{1}$$

and

$$\nabla^2 W-\mu\epsilon\frac{\partial^2 W}{\partial t^2}=0, \tag{2}$$

where $\overline{F}$ is any vector function of position and time, while W is any scalar function of position and time. If $\overline{F}$ is represented by

$$\overline{F}=\bar{u}_0U+\bar{v}_0V+\bar{w}_0W, \tag{3}$$

where $\bar{u}_0$, $\bar{v}_0$ and $\bar{w}_0$ are unit vectors, (1) gives

$$\begin{bmatrix} C_{11}-\mu\epsilon\frac{\partial^2}{\partial t^2} & C_{12} & C_{13} \\ C_{21} & C_{22}-\mu\epsilon\frac{\partial^2}{\partial t^2} & C_{23} \\ C_{31} & C_{32} & C_{33}-\mu\epsilon\frac{\partial^2}{\partial t^2}\end{bmatrix}\begin{bmatrix}U\\V\\W\end{bmatrix}=0, \tag{4}$$

where the C's are shorthand notations for various scalar differential operators as shown in the Appendix. An outstanding characteristic of the Cartesian coordinate system is that it gives $C_{11}=C_{22}=C_{33}=\nabla^2$, and all other C's are zero. In circular cylinder and spherical coordinates the vector wave equation becomes[2]

$$\begin{bmatrix} \nabla^2-\frac{1}{r^2}-\mu\epsilon\frac{\partial^2}{\partial t^2} & -\frac{2}{r^2}\frac{\partial}{\partial\phi} & 0 \\ \frac{2}{r^2}\frac{\partial}{\partial\phi} & \nabla^2-\frac{1}{r^2}-\mu\epsilon\frac{\partial^2}{\partial t^2} & 0 \\ 0 & 0 & \nabla^2-\mu\epsilon\frac{\partial^2}{\partial t^2}\end{bmatrix}\begin{bmatrix}F_r\\F_\phi\\F_z\end{bmatrix}=0, \tag{5}$$

and

$$\begin{bmatrix} \nabla^2-\frac{2}{r^2}-\mu\epsilon\frac{\partial^2}{\partial t^2} & -\frac{2}{r^2\sin\theta}\frac{\partial}{\partial\theta}\sin\theta & -\frac{2}{r^2\sin\theta}\frac{\partial}{\partial\phi} \\ \frac{2}{r^2}\frac{\partial}{\partial\theta} & \nabla^2-\frac{1}{r^2\sin\theta}-\mu\epsilon\frac{\partial^2}{\partial t^2} & -\frac{2\cos\theta}{r^2\sin^2\theta}\frac{\partial}{\partial\phi} \\ \frac{2}{r^2\sin\theta}\frac{\partial}{\partial\phi} & \frac{2\cos\theta}{r^2\sin^2\theta}\frac{\partial}{\partial\phi} & \nabla^2-\frac{1}{r^2\sin^2\theta}-\mu\epsilon\frac{\partial^2}{\partial t^2}\end{bmatrix}\begin{bmatrix}F_\eta\\F_\theta\\F_\phi\end{bmatrix}=0. \tag{6}$$

It is theoretically possible to determine the nine elements of any 3×3 G-matrix, consisting of scalar differential operators, such that $[G]\times[C]\times[G]_t$ gives a diagonalized matrix of scalar differential operators; $[G]_t$ is the transposition of $[G]$. However, the actual steps to determine the G-matrix appear extremely difficult. Instead, a simpler aspect of the C-matrix is pursued in this note.

If U and V are both zero, (4) becomes

$$C_{13}W=0,$$

$$C_{23}W=0,$$

and

$$\left[C_{33}-\mu\epsilon\frac{\partial^2}{\partial t^2}\right]W=0. \tag{7}$$

The question raised here is: "What types of coordinate systems satisfy (7)?" Having gone through the indicated differentiations of (7), one finds the answer to be that (1) be-

* Received March 23, 1962.

[1] J. A. Stratton, "Electromagnetic Theory," McGraw-Hill Book Co., Inc., New York, N. Y., pp. 49–50; 1941.
[2] P. M. Morse and H. Feshbach, "Methods of Theoretical Physics," McGraw-Hill Book Co., Inc., New York, N. Y., vol. 1, p. 116; 1953.
[3] P. Moon and D. E. Spencer, "Field Theory for Engineers," D. Van Nostrand Co., Inc., Princeton, N. J., pp. 81–84; 1960.

comes (2) if the metric coefficients are such that,

$$\frac{\partial l}{\partial w} = \frac{\partial m}{\partial w} = \frac{\partial n}{\partial u} = \frac{\partial n}{\partial v} = 0. \tag{8}$$

Actually (8) was initially obtained to satisfy the first two equations of (7). However, (8) happens to make C_{33} equal to the Laplacian operator.

The scalar wave equation is separable in eleven orthogonal curvilinear coordinate systems, and simple checks on these systems reveal that only five of them meet (8). They are Cartesian, circular cylinder, elliptic cylinder, parabolic cylinder, and bipolar coordinates. All five systems have $n=1$. No matter which two vector components are selected to be zero, (6) never gives a scalar wave equation in the spherical coordinate system. In contrast, if F_r and F_ϕ are selected to be zero, (5) provides a scalar wave equation of F_z in a cylindrical coordinate system. Spherical and conical coordinate systems have $l=1$, hence $\partial l/\partial w=0$, but these two systems do not satisfy the remaining equations of (8). The scalar Helmholtz wave equation is separable in six coordinate systems,[4] which are the first four of the five mentioned above plus spherical and conical coordinate systems. The transverse vector Helmholtz wave equation is also separable in these six coordinate systems.

It should be emphasized that (8) has been derived for a general scalar function, $W(u, v, w, t)$. If W is a specialized function of position, *i.e.*, if it is symmetric with respect to any coordinate, a weaker set of requirements for the metric coefficients results even if $U=V=0$ and (7) is met.

Finally, another application of (8) is in order for any $\overline{F}$ having nonzero U, V, and W. Eq. (4) shows that each vector component of (1) entails U, V, and W. A previous note[5] proved noncommutability between medium parameters and vector differential operators in Maxwell's equations if μ and ϵ are functions of position. The operators involved here are scalar differential operators. Therefore, operators and parameters commute and eliminations of U and V from (1) result in

$$\left[\left\{C_{31}\left(C_{22}-\mu\epsilon\frac{\partial^2}{\partial t^2}\right)-C_{21}C_{32}\right\}\left\{C_{21}C_{13}-C_{23}\left(C_{11}-\mu\epsilon\frac{\partial^2}{\partial t^2}\right)\right\}-\left\{C_{21}C_{12}-\left(C_{11}-\mu\epsilon\frac{\partial^2}{\partial t^2}\right)\left(C_{22}-\mu\epsilon\frac{\partial^2}{\partial t^2}\right)\right\}\left\{C_{31}C_{23}-C_{21}\left(C_{33}-\mu\epsilon\frac{\partial^2}{\partial t^2}\right)\right\}\right]W=0. \tag{9}$$

If the special requirements (8) are permitted, (9) reduces to

$$C_{21}\left(C_{33}-\mu\epsilon\frac{\partial^2}{\partial t^2}\right)\left\{C_{12}C_{21}-\left(C_{11}-\mu\epsilon\frac{\partial^2}{\partial t^2}\right)\cdot\left(C_{22}-\mu\epsilon\frac{\partial^2}{\partial t^2}\right)\right\}W=0, \tag{10}$$

which is a factorized form for $W(u, v, w, t)$. At most, a fourth-order linear partial differential equation is to be solved, while it had previously been thought that a six-order partial differential equation must be solved for similar cases.[4] Evidently, analyses of the peculiarities of the metric coefficients can save some labor in solving general vector wave equations in the above-mentioned five curvilinear orthogonal coordinate systems.

Appendix
Table of C's, Scalar Differential Operators

$$C_{11}: \frac{1}{l}\frac{\partial}{\partial u}\left(\frac{1}{lmn}\right)\frac{\partial}{\partial u}(mn\ )+\frac{1}{mn}\left[\frac{\partial}{\partial v}\left(\frac{n}{lm}\right)\frac{\partial}{\partial v}(l\ )+\frac{\partial}{\partial w}\left(\frac{m}{ln}\right)\frac{\partial}{\partial w}(l\ )\right]$$

$$C_{12}: \frac{1}{l}\frac{\partial}{\partial u}\left(\frac{1}{lmn}\right)\frac{\partial}{\partial v}(ln\ )-\frac{1}{mn}\left[\frac{\partial}{\partial v}\left(\frac{n}{lm}\right)\frac{\partial}{\partial u}(m\ )\right]$$

$$C_{13}: \frac{1}{l}\frac{\partial}{\partial u}\left(\frac{1}{lmn}\right)\frac{\partial}{\partial w}(lm\ )-\frac{1}{mn}\left[\frac{\partial}{\partial w}\left(\frac{m}{ln}\right)\frac{\partial}{\partial u}(n\ )\right]$$

$$C_{21}: \frac{1}{m}\frac{\partial}{\partial v}\left(\frac{1}{lmn}\right)\frac{\partial}{\partial u}(mn\ )-\frac{1}{ln}\left[\frac{\partial}{\partial u}\left(\frac{n}{lm}\right)\frac{\partial}{\partial v}(l\ )\right]$$

$$C_{22}: \frac{1}{m}\frac{\partial}{\partial v}\left(\frac{1}{lmn}\right)\frac{\partial}{\partial v}(ln\ )+\frac{1}{ln}\left[\frac{\partial}{\partial u}\left(\frac{n}{lm}\right)\frac{\partial}{\partial u}(m\ )+\frac{\partial}{\partial w}\left(\frac{l}{mn}\right)\frac{\partial}{\partial w}(m\ )\right]$$

$$C_{23}: \frac{1}{m}\frac{\partial}{\partial v}\left(\frac{1}{lmn}\right)\frac{\partial}{\partial w}(lm\ )-\frac{1}{ln}\left[\frac{\partial}{\partial w}\left(\frac{l}{mn}\right)\frac{\partial}{\partial v}(n\ )\right]$$

$$C_{31}: \frac{1}{n}\frac{\partial}{\partial w}\left(\frac{1}{lmn}\right)\frac{\partial}{\partial u}(mn\ )-\frac{1}{lm}\left[\frac{\partial}{\partial u}\left(\frac{m}{ln}\right)\frac{\partial}{\partial w}(l\ )\right]$$

$$C_{32}: \frac{1}{n}\frac{\partial}{\partial w}\left(\frac{1}{lmn}\right)\frac{\partial}{\partial v}(ln\ )-\frac{1}{lm}\left[\frac{\partial}{\partial v}\left(\frac{l}{mn}\right)\frac{\partial}{\partial w}(m\ )\right]$$

$$C_{33}: \frac{1}{n}\frac{\partial}{\partial w}\left(\frac{1}{lmn}\right)\frac{\partial}{\partial w}(lm\ )+\frac{1}{lm}\left[\frac{\partial}{\partial u}\left(\frac{m}{ln}\right)\frac{\partial}{\partial u}(n\ )+\frac{\partial}{\partial v}\left(\frac{l}{mn}\right)\frac{\partial}{\partial v}(n\ )\right].$$

Iwao Sugai
ITT Federal Laboratories
Nutley, N. J.

[4] Morse and Feshbach, *op. cit.*, vol. 2, pp. 1760–1767.

[5] I. Sugai, "Operators for wave equations in general linear media," IRE Trans. on Antennas and Propagation (*Communications*), vol. AP-9, pp. 501–502; September, 1961.

Second-Order Constancy of the One-Way Velocity of Light*

The possibility of a second-order variation in the one-way velocity of light has recently been discussed.[1] A variation in the one-way velocity of light to any order disagrees with the special theory of relativity and theoretically permits detection of an ether and measurement of absolute motion. Such a variation contradicts Ives' proof[2] that in the contraction theory (assumption of Newtonian space-time and existence of an ether) the one-way velocity of light is, in agreement with relativity, constant to all orders for a terrestrial nonrotating measurement. For a terrestrial rotating experiment, it has been shown that the predicted one-way velocity of light in the contraction theory is also constant and in agreement with relativity to the first order.[3,4] This is extended here to the second order.

Clocks are situated on a turntable at R and A, as shown in Fig. 1. For high sensitivity, a Mössbauer radiator and absorber may

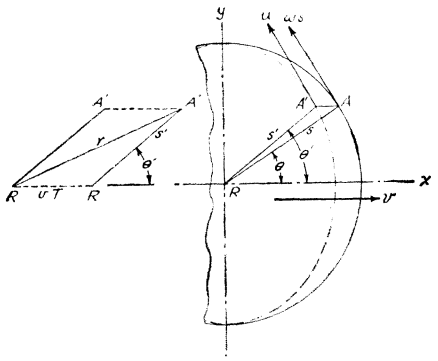

Fig. 1—Arrangement for the one-way measurement of the velocity of light.

be used as the clocks. If the table is moving with velocity v with respect to an observer outside the table, the table appears elliptical, as shown by the dashed curve, with the minor axis contracted by the factor $(1-\beta^2)^{1/2}$ in the direction of v, where β is v/c and c is the velocity of light in the medium between R and A. The clock at A appears to be at A'. If we assume an observer at rest in an ether, v becomes the velocity of the turntable through the ether. During the time T that is required for radiation to travel one-way (from R to A'), as measured by the observer, the turntable moves a distance vT in the ether. Since

$$T = r/c \tag{1}$$

and

$$r = (s'^2 + v^2T^2 + 2s'vT\cos\theta')^{1/2}, \tag{2}$$

* Received April 5, 1962.

[1] P. M. Rapier, "A proposed test for the existence of a Lorentz-invariant aether," Proc. IRE, vol. 50, pp. 229–230; February, 1962.

[2] H. E. Ives, "The measurement of the velocity of light by signals sent in one direction," *J. Opt. Soc. Am.*, vol. 38, pp. 879–884; October, 1948.

[3] M. Ruderfer, "First-order terrestrial ether drift experiment using the Mössbauer radiation," *Phys. Rev. Lett.*, vol. 5, pp. 191–192, September 1, 1960; see also "Erratum," vol. 7, p. 361, November 1, 1961.

[4] M. Ruderfer and P. M. Rapier, "A proposed test of the constancy of the velocity of light" (*Correspondence*) Proc. IRE, vol. 50, pp. 1700–1703; July, 1962.

where r, s' and θ' are as shown in Fig. 1, then the one-way light travel-time is

$$T = \frac{s'[\beta \cos\theta' + (1 - \beta^2 \sin^2\theta')^{1/2}]}{c(1 - \beta^2)}. \quad (3)$$

The effect of aberration has been automatically included in this expression by the method of derivation.

The turntable is assumed to rotate slowly with a uniform angular velocity $\omega = d\theta/dt$, *i.e.*, $v \gg \omega s$, such that error introduced by the rotation of A' during time T is negligible. The light travel-time T varies periodically with the rotation. This produces a variation in the phase of the radiation arriving at A' which appears as a frequency change. The frequency shift due to phase variation is

$$(\Delta f)_{ph} = -f_R dT/dt \quad (4)$$

where f_R is the frequency at R as measured by the observer. Differentiating (3) and substituting in (4) gives the relative frequency shift due to the phase variation

$$\left(\frac{\Delta f}{f_R}\right)_{ph} = \frac{\omega' s' \beta \sin\theta'}{c(1 - \beta^2)}\left[1 + \frac{\beta \cos\theta'}{(1 - \beta^2 \sin^2\theta')^{1/2}}\right] - \frac{ds'}{dt}\left[\frac{\beta \cos\theta' + (1 - \beta^2 \sin^2\theta')^{1/2}}{c(1 - \beta^2)}\right]. \quad (5)$$

If the distance s between R and A is s_0 when the table is at rest in the ether ($\omega = v = 0$), then s may be expressed as ks_0 when the table is uniformly rotated but not translated, where $1 > k > 0$ and k is a function of ω only. Radial symmetry is preserved. When the table is translated but not rotated, the elliptical shape is required by the contraction theory. The table distortion, in the contraction theory, due to combined rotation and translation has been discussed[5] but never completely solved. For $v \gg \omega s$, which is assumed here, the use of an elliptical shape does not lead to sensible error. Consequently, from the geometry

$$s' = s(1 - \beta^2 \cos^2\theta)^{1/2} \quad (6)$$

so that

$$\frac{ds'}{dt} = \frac{s\omega\beta^2 \sin\theta \cos\theta}{(1 - \beta^2 \cos^2\theta)^{1/2}}. \quad (7)$$

Also with the aid of the geometry

$$\cos\theta' = (1 - \beta^2)^{1/2}(1 - \beta^2 \cos^2\theta)^{-1/2} \cos\theta \quad (8)$$

$$\sin\theta' = (1 - \beta^2 \cos^2\theta)^{-1/2} \sin\theta \quad (9)$$

and

$$\omega' = d\theta'/dt = (1 - \beta^2)^{1/2}(1 - \beta^2 \cos^2\theta)^{-1}\omega. \quad (10)$$

In the contraction theory, the frequency of the clock at R is

$$f_R = f_0(1 - \beta^2)^{1/2} \quad (11)$$

where f_0 is the frequency of the clock at R when at rest in the ether. Substituting (6)–(11) in (5) we get the frequency shift due to phase variation

$$(\Delta f/f_0)_{ph} = (\omega s/c)\beta \sin\theta. \quad (12)$$

This is the result originally obtained as a first-order approximation for a rigid table,[3] but is derived here exactly for a slowly rotating table. Effects of translation in the ether on aberration and table dimensions have canceled.

The variation of clock frequency at A' with motion remains to be considered.[6] In the contraction theory, the frequency of the clock at A' is

$$f_A' = f_0[1 - (v_A'/c)^2]^{1/2} \quad (13)$$

where v_A' is the absolute velocity of A'. This is

$$v_A' = |v + u| = [(v + u_x)^2 + u_y^2]^{1/2} \quad (14)$$

where u is the velocity of A' with respect to the center of the ellipse. From the geometry of the ellipse

$$u_x = dx/dt = -\omega s(1 - \beta^2)^{1/2} \sin\theta \quad (15)$$

and

$$u_y = dy/dt = \omega s \cos\theta. \quad (16)$$

The relative frequency difference between clocks at R and A' is then

$$\left(\frac{\Delta f}{f_0}\right)_{cl} = \frac{f_A' - f_R}{f_0} = [1 - \beta^2 + 2(\omega s/c)\beta(1 - \beta^2)^{1/2} \sin\theta - (\omega s/c)^2(1 - \beta^2 \sin^2\theta)]^{1/2} - (1 - \beta^2)^{1/2}. \quad (17)$$

Dropping terms of higher order than $\omega\beta^2$ and ω^3, we get

$$(\Delta f/f_0)_{cl} = (\omega s/c)\beta \sin\theta - \tfrac{1}{2}(\omega s/c)^2. \quad (18)$$

The second term, sometimes referred to as the transverse Doppler shift, has previously been predicted by the contraction[7] and relativity theories. The first term cancels the effect in (12) due to variation in phase shift. The experiment should therefore give a null result regarding the detection of an ether to at least the second order in v. Because no second-order periodic effect is observable, a shift in clock positions or placement of the observer on the turntable or on a moving platform cannot give an observable second-order effect. The existence of the higher-order terms is not necessarily significant since the effects of accelerated motion due to rotation are ignored in obtaining (12).

The arrangement in Fig. 1 has been used at Harwell[8] to detect the second term of (18). The original objection[3] to this arrangement for the measurement of (12) may be obviated by continuously recording the frequency shift to correlate it with the orientation of the turntable in space.[9] Without such recording, the measurement available is the change in frequency shift as the earth's orientation in space varies. Sensitivity is then low because of the low angular velocity of the earth. Continuous recording preserves the full sensitivity obtained with the higher table rotation. The maximum frequency shift variation obtained in the Harwell experiment thus provides an upper limit to an ether drift. For a reported frequency shift from an ether drift <10 per cent of the change observed ($\Delta f/f_0 < 10^{-13}$), $s = 5$ cm and $\omega = 2\pi 500$ radian/sec, then for $\sin\theta = 1$, the maximum possible ether drift is less than 100 m/sec.[10]

This value is too low to contain an actual ether drift due to translation of the earth through an ether. The experiment supports the previous conclusion that the existence of an ether is not detectable by macroscopic means.[11] However, because the surface velocity of the earth at Harwell is also about 100 m/sec, the observed frequency-shift variation may be due, in part, to rotational effects, gravitational effects on the one-way velocity of light, or other causes. It is consequently of interest to extend the theory to include acceleration effects due to rotation.

MARTIN RUDERFER
Dimensions, Inc.
Brooklyn 4, N. Y.

[5] H. E. Ives, "Theory of the double Fizeau toothed wheel," *J. Opt. Soc. Am.*, vol. 29, pp. 472–478; November, 1939.

[6] The omission in the original reports of the effect of clock motion[3,4] was first called to the author's attention by F. J. Belinfante in a letter dated October 15, 1960, wherein he calculated the clock correction by use of the time transformation formula from Lorentz's pre-relativistic dynamical contraction theory.

[7] H. E. Ives, "The Doppler effect considered in relation to the Michelson-Morley experiment," *J. Opt. Soc. Am.*, vol. 27, pp. 389–392; November, 1937.

[8] H. J. Hay, J. P. Schiffer, T. E. Cranshaw, and P. A. Egelstaff, "Measurement of the red shift in an accelerated system using the Mossbauer effect in Fe^{57}," *Phys. Rev. Lett*, vol. 4, pp. 165–166; February 15, 1960.

[9] J. P. Schiffer, meeting with author; December 23, 1960.

[10] T. E. Cranshaw, private communication; July 8, 1960.

[11] M. Ruderfer, "Re-evaluation of the existence of an ether," PROC. IRE, vol. 50, pp. 325–326; March, 1962.

Bergeron's Graphic Method*

We read with great interest the article by Nagumo and Shimura.[1] The method they describe is quite familiar to us and is known as the "Bergeron Graphic Method." We felt some regret at seeing the name of Bergeron unmentioned and must conclude that his work, though dating back to 1931, is hardly known abroad, if at all.

His first book "Methodes Graphiques" was published in 1931. The method outlined therein is currently taught in the chief French engineering schools, *viz.*, at the Ecole Centrale by Bergeron himself, at the Institute Polytechnique (since 1942) in Grenoble by Esclangon and at the Ecole Supérieure d'Electricité, by M. Cahen. Another book by Bergeron[2] sets forth this method and gives many typical examples as applied to the engineering arts.

The method was reapplied systematically in the chapter dealing with nonlinear elements associated with transmission lines. This chapter is part of the course on transmission lines as taught at the Compagnie des Machines Bull. You will find below an excerpt from the above-mentioned course, which endeavours to set forth the method concisely.

* Received January 16, 1962; revised manuscript received, February 15, 1962.

[1] J. Nagumo and M. Shimura, "Self-oscillation in a transmission line with a tunnel diode," PROC. IRE, vol. 49, pp. 1281–1291; August, 1961.

[2] L. Bergeron, "Du Coup de Belier en Hydraulique au Coup de Foudre en Électricité," Messrs. Dunod, Paris, France; 1950.

Broadly speaking the method is applicable to any problem amenable to propagation equations of the "vibrating reed" type such as:

$$\frac{\partial^2 f}{\partial x^2} = \frac{1}{u^2}\frac{\partial^2 f}{\partial t^2}, \tag{1}$$

where f is a function of the spatial coordinate x and the time t, u being the velocity of propagation. As is well known, such an equation governs propagation of acoustic waves in solids, propagation of electric waves along power transmission lines (disturbances due to lightning surges on a line, to a short circuit, or the like), propagation of electromagnetic transverse waves in waveguides and transmission lines, propagation of shock waves in penstocks of hydraulic plants and many other phenomena.

The solution of the equation takes the form

$$f(x, t) = g(x - ut) + h(x + ut) \tag{2}$$

and comprises two terms corresponding to two waves propagating in opposite directions at the velocities u and $(-u)$.

Assume a lossless transmission line and $i(x, t)$, $v(x, t)$ the current and voltage at a point of the line along the abcissa x and at time t. Since

$$v(x, t) = g(x - ut) + h(x + ut), \tag{3}$$

$$i(x, t) = \frac{1}{R_c}[g(x - ut) - h(x + ut)], \tag{4}$$

R_c being the wave resistance of the lossless line.

Let us now consider an observer O_1, moving at the velocity $+u$, found at the point $x = x_0$ at the instant $t = 0$. (See Fig. 1.)

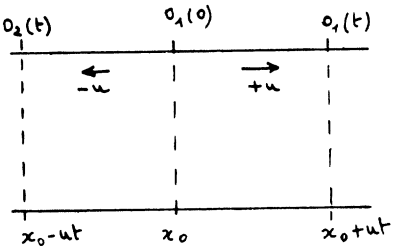

Fig. 1.

At that instant, he observes the voltage and the current

$$v_0 = v(x, 0) = g(x_0) + h(x_0), \tag{5}$$

$$i_0 = i(x, 0) = \frac{1}{R_c}[g(x_0) - h(x_0)]. \tag{6}$$

At any instant t, he will be at the abscissa point $x = (x_0 + ut)$ and observes the voltage

$$v[(x_0 + ut), t] = g[(x_0 + ut) - ut] + h[(x_0 + ut) + ut] \tag{7}$$

$$= g(x_0) + h(x_0 + 2ut), \tag{8}$$

and the current

$$i[(x_0 + ut), t] = \frac{1}{R_c}[g(x_0) - h(x_0 + 2ut)]. \tag{9}$$

The voltage variation observed between the instant $t = 0$ at the point x_0 and the instant t at the point $(x_0 + ut)$, his present position, is

$$\Delta v_1 = v[(x_0 + ut), t] - v(x_0, 0) = h(x_0 + 2ut) - h(x_0). \tag{10}$$

The variation of the current being

$$\Delta i_1 = i[(x_0 + ut), t] - i(x_0, 0) = -\frac{1}{R}[h(x_0 + 2ut) - h(x_0)], \tag{11}$$

it being observed that

$$\boxed{\Delta v_1 = -R_c \Delta i_1}. \tag{12}$$

Hence, for the observer, moving at the velocity $(+u)$, the voltage and current variations appear as being in the ratio $(-R_c)$.

This has a graphic interpretation, as follows: plot in the plane (v, i) the voltage and current of the line along two mutually perpendicular axes. At the instant $t = 0$, the observer had observed v_0 and i_0, the condition of the line being denoted by the point P.

At any instant t, the voltage v and the current i he observes are such that the variations Δv and Δi satisfy the equation

$$\Delta v = -R_c \Delta i.$$

The point showing the condition of the line observed by O_1 generates as a straight line D_1, the slope of which is $-R_c$ (see Fig. 2). Let us now consider a second observer O_2 moving at the velocity $(-u)$ and at the point $x = x_0$ at the time $t = 0$.

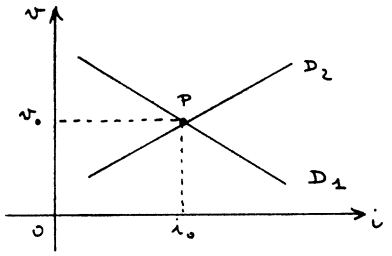

Fig. 2.

When $t = 0$ the voltage and current are

$$v(x_0, 0) = g(x_0) + h(x_0), \tag{13}$$

$$i(x_0, 0) = \frac{1}{R_c}[g(x_0) - h(x_0)]. \tag{14}$$

At the instant t, the voltage and current observed are

$$v[(x_0 - ut), t] = g(x_0 - 2ut) + h(x_0), \tag{15}$$

$$i[(x_0 - ut), t] = \frac{1}{R_c}[g(x_0 - 2ut) - h(x_0)]. \tag{16}$$

From the instant O to the instant t, the voltage and current variations observed are

$$\Delta v_2 = g(x_0 - 2ut) - g(x_0), \tag{17}$$

$$\Delta i_2 = \frac{1}{R_c}[g(x_0 - 2ut) - g(x_0)], \tag{18}$$

linked by

$$\boxed{\Delta v_2 = R_c \Delta i_2}. \tag{19}$$

Therefore, the point corresponding to the observations of O_2 generates a straight line, the slope of which is $(+R_c)$, and passing through P. (See Fig. 2.)

Conclusion

Bergeron's graphic method is highly suitable for analyzing linear, but even more so, nonlinear circuits based on transmission lines because it allows working with actual characteristics.

When the circuit includes reactive elements, the use of the method is more critical as the loci become more intricate, but there are no restrictions in principles to the use of the method.

Bergeron's book contains numerous examples of this latter type.

P. Chapouille
J. P. Vabre
Compagnie des Machines Bull.
Paris, France

Author's Comments[3]

We thank Messrs. Chaupouille and Vabre very much for their kindness in informing us of the existence of such an excellent book. Indeed, Bergeron's graphical method as described is quite comprehensive and involves the method of construction used in our paper.

Although, we cannot find in his book any treatment of "self-excited periodic oscillations," on which our main interest is focused, we would have made reference to his book if we had known of it.

J. Nagumo
M. Shimura
Dept. of Applied Physics,
Faculty of Engineering,
University of Tokyo,
Tokyo, Japan

[3] Received September 17, 1962.

Experiments on a Partially Shielded Ruby Laser Rod*

Past experiments on a pulsed ruby laser which have been reported in the literature were conducted with the full length of the rod, except for the portion in the clamping chuck, exposed to pumping radiation. Assuming that the population in the metastable level is proportional to the input energy, the condition for laser action at constant temperature in these cases may be written [1], [2]

$$E_T l = K\left(\ln\frac{1}{R} + \beta l\right), \tag{1}$$

where E_T = input energy at threshold, l = length of rod, K = a constant, R = reflec-

* Received August 30, 1962.

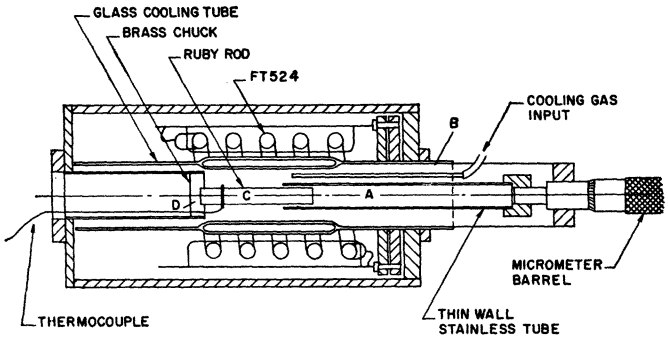

Fig. 1—Drawing of the laser head used for the shielding experiments.

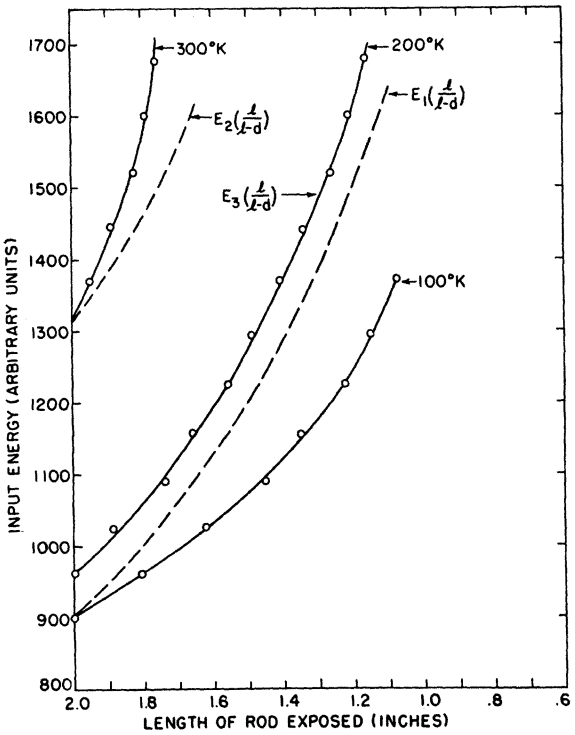

Fig. 2—Threshold energy vs length of rod exposed. The parameters E_1, E_2, and E_3 represent the threshold energy when the full length of the rod is pumped. The dotted lines represent the calculated pumping energy assuming no loss and the solid lines were determined from experimental data as shown.

tivity of the cavity ends, and βl = scattering loss in the laser rod.

In this experiment, the ruby rod was held from one end and positioned in the center of the FT-524 laser head as shown in Fig. 1. The laser head was equipped for cooling to 77°K and a thermocouple was securely attached to the ruby rod to measure the temperature. A close fitting cylindrical light shield of thin-walled stainless steel tubing was slipped over the end of the rod from the end opposite the suspension chuck and positioned along the rod with a micrometer screw. The ruby rod employed was of 0.05 per cent Cr^{3+} concentration, $\frac{1}{4}$ inch diameter, 2 inch length and 90° orientation with $\frac{1}{2}$ per cent transmitting end coatings.

In order to determine the effect of pumping light entering around the end of the light shield, a simple experiment was performed. An aluminum-foil shield of one-half the length of the rod was slipped over the end of the rod, the shield was cut in half, then into four sections giving the same total length and the threshold measured in each case. The case with eight ends differed from the case with two ends by only 3 per cent.

With a length d of the rod shielded from pumping radiation, the threshold equation becomes

$$E_T(l - d) = K(\ln 1/R + \beta l + \gamma d), \quad (2)$$

where γ is the effective absorption coefficient in the shielded part of the rod.

Observations of the threshold energy as a function of the length of the rod exposed to pumping radiation are shown in Fig. 2 for three different values of temperature. If the shielded portion of the rod caused no absorption loss, one would expect the threshold to increase with the length of rod shielded as $l/l\text{-}dE_0$, where E_0 is the threshold energy when the full rod is exposed. When the shielded portion of the rod introduces gain, the measured threshold curve should lie below a curve $l/l\text{-}d$ and when the shielded portion of the rod introduces loss, the measured curve should lie above the $l/l\text{-}d$ curve. All three of these cases are shown in Fig. 2.

Measurements at 300°K indicate that the shielded portion of the rod introduces loss in the cavity. This corresponds to the condition $B\rho < (1/\tau)$ where B = Einstein coefficient for induced transitions, ρ = power per unit frequency interval and τ = fluorescence lifetime. Data taken at 200°K indicate that no loss is introduced by the shielded portion of the rod and corresponds to the situation where the absorption coefficient is saturated. Measurements at 100°K indicate that the shielded part of the rod introduces gain. This result is completely incompatible with fluorescent energy transfer by absorption and at the present time the transfer mechanism is not understood. These results do show, however, that the pumping efficiency for a pulsed ruby laser can be increased up to 20 per cent at temperatures below 200°K by increasing the pumping energy per unit length and reducing the length pumped.

The writer wishes to thank Dr. D. Chen and J. F. Ready for informative discussions and D. L. Hardwick for assistance in designing the laser head and taking the data.

R. L. Aagard
Honeywell Res. Ctr.
Hopkins, Minn.

References

[1] A. L. Schawlow, "Infrared and optical masers," *Solid State J.*, vol. 2, pp. 21–29; June, 1961.
[2] R. L. Aagard, "Measurements of the output from a pulsed ruby laser with central hole in one of the end mirrors," *J. Appl. Phys.*, vol. 33, pp. 2842–2844; September, 1962.
[3] A. L. Schawlow, "Fine structure and properties of chromium fluorescence in aluminum and magnesium," in "Advances in Quantum Electronics," J. R. Singer, Ed., Columbia University Press, New York, N. Y., p. 50; 1961.

Redistribution of Stimulated Emission Energy in Ytterbium Activated Glass Etalons*

The purpose of this communication is to describe the time dependence of stimulated emission from ytterbium activated glass optical resonators and how this emission has been influenced by the surface conditions of the etalons. Stimulated emission from ytterbium activated silicate glass and some of its characteristics have been reported previously.[1] In the present work, the glass etalons were of the Fabry-Perot type and were 4 mm in diameter and 27 mm long; the ends of the rods were coated with evaporated silver metal, one end to about two per cent transmission, the other end to opacity. The lithium-magnesium-aluminosilicate glass contained one cationic mole per cent of ytterbium; this ion exhibits stimulated emission in a narrow band of wavelengths centered around 1.015μ. In the apparatus used in this work, essentially all of the radiation emanating from the

* Received September 11, 1962.
[1] H. W. Etzel, H. W. Gandy, and R. J. Ginther, "Stimulated emission of infrared radiation from ytterbium activated silicate glass," *Applied Optics*, vol. 1, pp. 534–536; July, 1962.

transmitting end of the etalon is collected and measured, so that the oscilloscopic traces shown represent the time dependence of the spatially integrated resonator output; a spatial analysis of the etalon emission with this experimental arrangement is not feasible.

The emission from a low concentration ytterbium activated glass etalon is shown in Fig. 1(a); comparison of the two traces shows that no stimulated emission has taken place and that the etalon signal trace consists of stray flashtube radiation and the long-lived ytterbium spontaneous emission. The lifetime for this emission has been determined to be 1.5 msec. The radiation output of a higher concentration (one mole per cent) Yb activated glass etalon with a highly polished cylindrical surface is shown in Fig. 1(b). The most noteworthy feature of the signal trace here is the rather large hump which appears approximately 800 μsec after the peak in the excitation trace; the spontaneous emission lifetime for Yb in this glass is also 1.5 msec. The qualitative character of the signal trace from this etalon did not change even when excited by a fifty per cent larger flashtube pulse. However, when this etalon is excited either at much lower excitation energies with the reflecting films intact, or at the highest excitation energies possible in our equipment ($\sim$5000 joules) but with a small part of the total reflecting film removed, then the oscilloscopic trace which occurs is of the type shown in Fig. 1(a).

The output trace of the same etalon when excited in the same way with the same flashtube input energy (as for Fig. 1(b)) but with the cylindrical surface now roughened is shown in Fig. 1(c). In addition to a hump which again occurs with the same 800-μsec delay as before, there now appear spikes superimposed on this hump; the threshold for spiking in this etalon occurs at an excitation level about ten per cent lower than that used in obtaining the trace in Fig. 1(c).[2] However, the roughened-surface etalon exhibits heavier spiking action which occurs earlier in the excitation pulse as higher excitation energies are used. The roughened-surface etalon also exhibits a trace similar to Fig. 1(a) under the same auxiliary experimental conditions mentioned above for the polished-surface etalon. It is important to note here that the optical quality of the glass in this etalon is only fair as indicated by its rather high threshold for laser action; for example, another etalon of this glass composition whose optical quality was visually judged to be better than the one reported above had a threshold for spiking some $2\frac{1}{2}$ times lower. The effects described above have also been observed in etalons fabricated from silicate glass samples which have been melted either in oxidizing or reducing atmospheres and at several activator concentrations; hence it is believed that the changes in the pattern of the emission traces do not depend critically upon the details of glass preparation when the active medium of the etalon is optically inhomogeneous.

The observation that the delayed optical outputs shown in Fig. 1(b) and (c) can be eliminated by partially removing the totally reflecting film suggests that these traces are not merely due to single-pass amplification of spontaneous emission. Furthermore, it would seem that those cavity modes which involve specular reflection at the highly-polished cylindrical surface of the etalon dominate in the trace in Fig. 1(b); hence in this etalon, it appears that such nonaxial ("humping") modes compete favorably for the distribution of stimulated emission possibly because they may have lower thresholds. When the specular reflecting character of the cylindrical surface of the etalon is destroyed, and the etalon is excited to the same level using the same nonfocused excitation scheme, the spiking associated with axial modes receives a larger share of the luminescent energy stored in the etalon. It should be noted that in the oscilloscopic trace, some of the hump still remains indicating that some of the low-threshold off-axis modes are still active; these nonaxial modes are likely to be those whose angles of incidence at the cylindrical surface are large and those in which the diminished projected surface roughness allows something approaching specular reflection to take place. However, even these off-axis modes apparently are attenuated by the surface condition as suggested by the observation that at higher excitation energies the axial modes grow much more rapidly than do the nonaxial modes. It would then seem that roughening the cylindrical surface of the etalon has the net effect of redistributing the stimulated emission energy from the nonaxial class of modes to the axial class of modes.

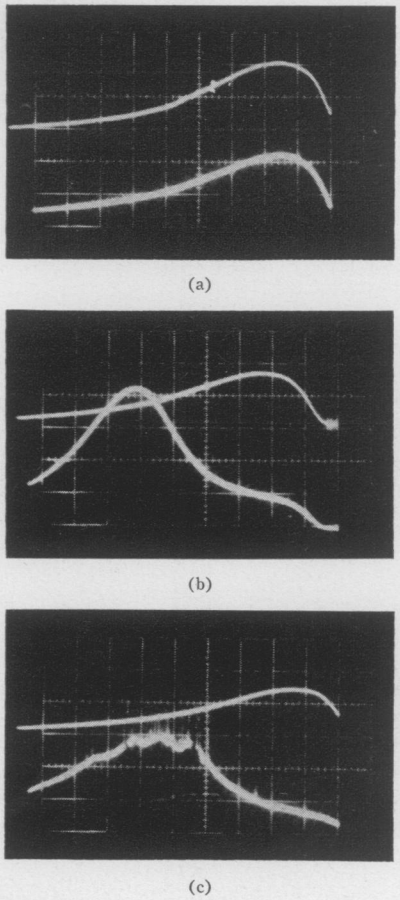

Fig. 1—Stimulated emission from ytterbium activated silicate glass at 78° k. Detector band pass 1.0–1.4μ; excitation source, GE FT-524 Xenon Flashtube, 450 μf capacitance; 200 μsec per division. Top trace in each picture: time variation of excitation intensity. (a) Emission from 0.1 per cent Yb glass etalon. No stimulated emission observed. Electrical input energy to lamp, 4400 joules. (b) Emission from 1.0 per cent Yb glass etalon; highly polished cylindrical surface. Electrical input energy to lamp, 3400 joules. (c) Emission from the 1.0 per cent glass etalon shown in (b) except the cylindrical sides have been roughened. Individual pit size in the cylindrical surface varied from 20 to 40μ in size. Electrical input energy to lamp, 3400 joules.

The conclusion reached here can be qualitatively understood within the framework of the multimode cavity theory given by Wagner and Birnbaum.[3] Because of the poor optical quality of etalons used in this work, the assumption of noncoupled modes made in this theory preclude its detailed correlation with present work. Nevertheless, the results given here agree with these writers' contention that stimulated emission energy in a multimode cavity is shifted from high loss rate modes into high Q modes as the excitation energy is increased.

The nature of the oscilloscopic traces shown here in Fig. 1(b) and (c) have been of significant use in the interpretation of oscilloscopic traces obtained from doubly activated (Yb and Nd) glass etalons, particularly the Yb component of the stimulated emission.[4]

The author is grateful to R. J. Ginther who prepared the experimental glasses and to R. J. Collins for several conversations relating to surface reflection modes. He is also grateful to C. C. Klick for helpful suggestions concerning the manuscript.

HAROLD W. GANDY
U.S. Naval Research Lab.
Washington, D.C.

[2] Although the detector gain was approximately the same for recording the bottom traces in Fig. 1(b) and (c), only the shape of these curves is being considered in this communication.

[3] W. G. Wagner and G. Birnbaum, "Theory of quantum oscillators in a multimode cavity," *J. Appl. Phys.*, vol. 32, pp. 1185–1194; July, 1961.

[4] H. W. Gandy and R. J. Ginther, "Simultaneous laser action of neodymium and ytterbium ions in silicate glass," PROC. IRE, vol. 50, pp. 2114–2115; October, 1962.

CdSe Photoconductive Field Effect Transistor*

Photoconductive field effect transistors have been successfully fabricated out of cadmium selenide, a group II-VI compound. These transistors have a mutual transconductance of 8 μmhos and a pinch-off voltage of 40 v at 100-μa drain current. The input impedance of these devices is 100 megohms. The transistors were fabricated from single crystal plates grown at this laboratory. The fabrication techniques were very similar to those employed in the construction of the cadmium sulfide field effect transistor.[1]

* Received August 22, 1962.

[1] R. R. Bockemuehl, "Cadmium sulfide field-effect phototransistor," PROC. IRE, vol. 48, pp. 875–882; May, 1960.

Indium was used for the source and drain contacts while copper is used for the gate.

The spectral characteristics were investigated and revealed a sharp dip in the pinch-off current at 7100 A which is shorter than the photocurrent excitation peak. This is thought to be an effect limited to the depletion region only. Infrared quenching illumination ($\lambda = 8000 - 14000$ A) influences the active characteristics of the transistor much more than it does the bulk photoconductance which indicates a dependence of hole drift mobility on infrared illumination similar to that exhibited by cadmium sulfide.[2]

These transistors are similar to those made from cadmium sulfide except for their photopeak which occurs at 7300 A and a temperature effect that reduces photocurrent as the temperature increases. The photocurrent change amounts to 3.6 per cent/°F in a region from −40 to +40°F. Beyond these limits it is much more stable. The copper impurities are sensitizing centers in cadmium selenide and lie about 0.6 ev above the valence band. At room temperature these centers have an almost equal probability of acting as recombination centers or as hole traps. This results in a strong dependence of carrier life time on both temperature and carrier density.[3]

JAMES W. BERGSTROM
Electronics and Instrumentation Dept.
General Motors Tech. Ctr.
Warren, Mich.

[2] R. R. Bockemuehl, J. E. Kauppila, and D. S. Eddy, "Analysis of photojunctions formed by diffusing copper into insulating cadmium sulfide crystals," *J. Appl. Phys.*, vol. 32, pp. 1324–1330; July, 1961.
[3] A. Rose, "Performance of photoconductors," PROC. IRE, vol. 43, pp. 1850–1869; December, 1955.

Iterative Procedures*

Consider the solution of a set of n linear algebraic equations in n unknowns

$$Ax - b = 0 \tag{1}$$

where A is a nonsingular square matrix of order n with (known) real elements a_{ij}; b and x are column vectors whose elements, b_j and x_j, represent the known and the unknown quantities.

We set

$$Ax - b = e \tag{2}$$

and form

$$x = Ke = K[Ax - b] \tag{3}$$

where K is a scalar multiplier as yet undetermined. Now, if the dynamical system defined by (3) is stable, its stationary point, $\dot{x} = 0$, implies a solution of (1). The elements of x are continuous functions of time, the elements of b are constants; taking the one-sided Laplace transform with $x(0) = 0$, we find the solution to (3) in the transform domain

$$\bar{X}(s) = \left[A - \frac{s}{K} I\right]^{-1} \frac{b}{s} \tag{4}$$

$$= \frac{A^{-1}b}{s}$$

$$+ \sum_{j=1}^{n} \lim_{s \to s_j} (s - s_j)\left[A - \frac{s}{K} I\right]^{-1} \frac{b}{s} \cdot \tag{4a}$$

We make the association

$$\lambda_j = \frac{s_j}{K}, \qquad j = 1, 2, \cdots, n; \tag{5}$$

if all of the eigenvalues, λ_j, of the matrix A have real parts of the same algebraic sign, we may choose K to be of opposite sign and assure system stability. If the matrix A is to be arbitrary, we replace (3) by

$$\dot{x} = KA^T e = KA^T[Ax - b]. \tag{6}$$

The matrix A^TA is the matrix associated with a positive definite quadratic form; all of its eigenvalues are real and obey

$$\lambda_j[A^TA] > 0. \tag{7}$$

The association of (5) implies stability of (6) for an arbitrary choice of A if K is chosen to be a negative scalar; increasing the magnitude of K merely speeds up the system. The system of (6) instruments the method of steepest descent of the quadratic surface defined by

$$E(x) = e^T e. \tag{8}$$

If the elements of x are discrete number sequences of argument m, the discrete equivalents of (2) and (3) are

$$Ax(m) - b = e(m) \tag{9}$$

$$x(m + 1) - x(m)$$

$$= Ke(m) = K[Ax(m) - b]. \tag{10}$$

Using the one-sided Z transform with $x(0) = 0$, we find

$$\bar{X}(Z) = \left[A - \frac{Z - 1}{K} I\right]^{-1} \frac{b}{1 - Z^{-1}} \cdot \tag{11}$$

The association equivalent to (5) is

$$Z_j = 1 + K\lambda_j, \quad j = 1, 2, \cdots, n. \tag{12}$$

In general the eigenvalues of the matrix A may be real or complex. In Fig. 1 they are indicated as lying within the circle of radius $K\lambda_{max}$ where λ_{max} is the maximum eigenvalue of the matrix A. The poles, Z_j, associated with the elements of the number sequence, $x(m)$, must lie within the unit circle in the Z plane if the dynamical system of (11) is to be stable. Given an arbitrary choice of A, little may be said regarding the stability of the system described by (10).

If we use the discrete equivalent of (6), we have

$$x(m + 1) - x(m) = KA^T[Ax(m) - b] \tag{13}$$

which transforms into

$$\bar{X}(Z)$$

$$= \left[A^TA - \frac{(Z - 1)}{K} I\right]^{-1} \frac{A^Tb}{1 - Z^{-1}} \cdot \tag{14}$$

The association of (12) still applies; because of the positive definiteness of the matrix

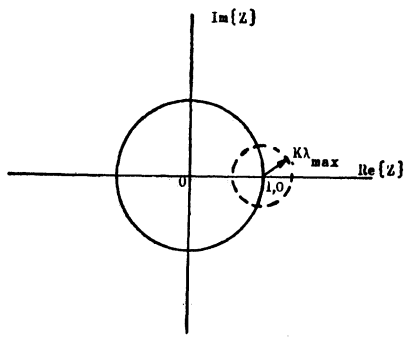

Fig. 1—Correspondence between $\lambda_j(A)$ and Z_j.

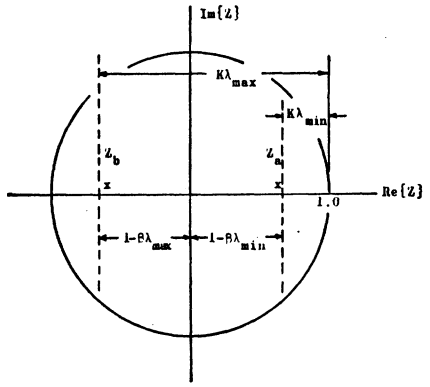

Fig. 2—Correspondence between $\lambda_j(A^TA)$ and Z_j.

A^TA, we require that the scalar multiplier be a negative real constant. The pole locations in the Z plane corresponding to $\lambda_{min}[A^TA]$ and $\lambda_{max}[A^TA]$ are represented by Z_a and Z_b in Fig. 2.

If we set $K = -\beta$ and position the poles corresponding to the slowest converging modes equidistant from the origin, we have

$$\beta = \frac{2}{\lambda_{max} + \lambda_{min}} \cdot \tag{15}$$

If we define

$$\mu_{[A^TA]} = \frac{\lambda_{max}[A^TA]}{\lambda_{min}[A^TA]}, \tag{16}$$

we find that the distances of Z_a and Z_b from the origin of the Z plane are

$$|Z_a| = |Z_b| = \frac{\mu - 1}{\mu + 1} \cdot \tag{17}$$

The rate of convergence is implicit in (17). The quantity μ is referred to as the conditioning number of a matrix. A well-conditioned matrix has $\mu \cong 1$. Since $\mu_{[A^TA]} = [\mu_A]^2$, we see that premultiplication by the matrix A^T assures us stability for an arbitrary choice of the A matrix but is not necessarily the most expedient, with respect to rate of convergence, method of iteration.

J. A. KNUDSON
Philco Corporation
Western Development Labs.
Palo Alto, Calif.

BIBLIOGRAPHY

[1] W. A. Adcock, "An automatic simultaneous equation computer and its use in solving secular equations," *Rev. Sci. Instr.*, vol. 19, pp. 181–187. March, 1948.
[2] G. A. Korn, "Stability of simultaneous equation solvers," PROC. IRE, vol. 37, pp. 1000–1002; September, 1949.

* Received June 7, 1962; revised manuscript received June 28, 1962.

Comment on "Double-Pumped X-Band Parametric Amplifier with Extremely Large Gain-Bandwidth Product"*

I have noted with interest the description by Spacek, in the above article,[1] of an X-band parametric amplifier which has had its gain-bandwidth product greatly increased through the use of two pump oscillators. Surely the resulting amplifier is a superregenerative amplifier operated with a novel technique for excitation and quenching of oscillations, rather than a new concept in parametric amplifiers.

To justify my view, it is necessary to consider the operation of a superregenerative parametric amplifier. In this amplifier, oscillations are periodically built up and quenched by periodic variation of one or more of the parameters governing oscillation; namely, pump level or frequency, diode bias, output loading. The use of a pump voltage on the diode, composed of the sum of two CW voltages separated in frequency by f will result in periodic quenching and build up of oscillations at a quench frequency f. Of course, this operation will require that the parameters of the parametric amplifier have been suitably adjusted for oscillation when the two CW pump voltages are in phase, and no oscillation when the two are in phase opposition.

At least three papers have been written discussing various properties of the parametric amplifier used as a superregenerative receiver[2-4] with one in particular[3] pointing out the increase in both gain and bandwidth in this mode, as compared with the conventional regenerative mode.

RICHARD F. CLARK
Radio and Elec. Engrg. Div.,
Nat'l Res. Council
Ottawa, Canada

* Received June 29, 1962.

[1] G. C. Spacek, PROC. IRE (*Correspondence*), vol. 50, pp. 1534–1535; June, 1962.

[2] B. B. Bossard, "Superregenerative reactance amplifier," PROC. IRE *Correspondence*), vol. 47, pp. 1269–1271; July, 1959.

[3] J. J. Younger, A. G. Little, H. Heffner, and G. Wade, "Parametric amplifiers as superregenerative detectors," PROC. IRE (*Correspondence*), vol. 47, pp. 1271–1272; July, 1959.

[4] B. B. Bossard, E. Frost, W. Fishbein, "X-band super-regenerative parametric amplifier," PROC. IRE. (*Correspondence*), vol. 48, pp. 1329–1330; July, 1960.

Author's Comment[5]

I have expected a comment similar to Mr. Clark's. However, his conclusion, although quick and very positive, is not correct. Surely a double-pumped parametric amplifier is not a superregenerative amplifier, but the equivalent of a large number of staggered tuned parametric amplifiers, where each hypothetical amplifier amplifies over a different frequency band such that the adjacent center frequencies of the individual bands are separated by the pump frequencies difference Δf, as will be shown in the theoretical paper mentioned in my note.[1]

[5] Received July 17, 1962.

The explanation that the double-pumped parametric amplifier is actually a superregenerative amplifier is the most obvious conclusion to be reached by an average engineer familiar with the state-of-the-art in parametric amplifiers and with the references given by Clark. Since I am an average engineer and familiar with the above references, I too have first thought that some superregeneration is responsible for the observed tremendous increase of gain and bandwidth, which was much larger than theoretically expected. For this reason, the double-pumped parametric amplifier was investigated as thoroughly as possible especially from this point of view. The results of this investigation showed that:

1) No discrete frequency spectrum (with the exception of pump frequencies) exists on the output of the amplifier in the absence of a coherent input signal. A superregenerative amplifier is essentially an ON-OFF oscillator, the oscillations of which are started sooner or later, depending on the input signal amplitude. Since the oscillations can be triggered also by thermal noise, the output of a superregenerative amplifier should contain discrete frequency components spaced in our case by the pump frequency separation (which would be the effective quench frequency) from each other even in the absence of a coherent input signal. However, no such spectrum was found, using one of the most sensitive spectrum analyzers available.

2) The superregenerative mode should manifest itself by substantial increase of the varactor dc current. No such increase was found.

3) The measured noise figure of the double-pumped parametric amplifier is either better or equal to the noise figure of the same parametric amplifier conventionally driven by one pump. It appears to me that superregeneration should substantially increase the noise figure, because of the high basic output power level, generated by the intermittent oscillations. The noise figure increase would be even more pronounced in the experimental set-up I have used, at which a low-power traveling-wave tube was used as the second-stage amplifier; if the double-pumped parametric amplifier were superregenerative amplifier, its oscillations power would saturate the TWT, thus increasing the over-all noise figure of the paramp-TWT receiver. See, for example, the paper by Bossard, *et al.*,[3] for the noise figure of a superregenerative parametric amplifier.

4) No critical adjustment of the phases of the two pump voltages are necessary as Clark perhaps assumes.

5) The gain-frequency characteristic of a double-pumped parametric amplifier is quite different from the gain-frequency characteristic of a superregenerative parametric amplifier. This was established by modifying one of the earlier low-frequency models of the DPPA into a superregenerative parametric amplifier. This amplifier used first two pumps at 18.6 Mc and 18.3 Mc, respectively. The 18.6 Mc pump was then replaced by a quenching oscillator at 300 kc, thus changing the amplifier into a superregenerative amplifier. The bandwidth was much smaller, however, in this latter case as compared with the double pumps drive.

6) The shape of the measured gain-frequency response of the DPPA correlates very well with the theoretically computed curves. The computed curves are based on a theory (not published as yet), which uses frequency folding rather than superregeneration as the basic idea of multiple pumping. This correlation makes me believe that I understand correctly the amplification mechanism of the DPPA.

To conclude, it appears to me that it should be possible to run a DPPA in the superregenerative mode. A multiple frequency spectrum was actually observed on the output of an amplifier even in the absence of a coherent input signal. However, this spectrum appears suddenly only if the pump drive is increased over certain level. This is a situation similar to the oscillation level of a conventional single-pump parametric amplifier, with the difference that DPPA oscillates not at one signal and one idler frequency only, but typically at 6 signal and idler frequencies simultaneously, depending on the Q's of the tanks and the pump separation Δf. The reason is that pure real input impedance is present at multiplicity of signal frequencies, in contrast with single-pump parametric amplifier, where pure resistive input impedance is present for one signal frequency only (excluding band-filter paramps). However, no gain measurements were ever made with the X-band DPPA at or just before the oscillation level, because the pump drive was not sufficient to approach this condition in the double-pumped case.

GEORGE C. SPACEK
P.O. Box 3671
Santa Barbara, Calif.

Further Comment on "Double-Pumped *X*-Band Parametric Amplifier with Extremely Large Gain-Bandwidth Product"[6]

A recent letter[1] to the IRE reported rather startling improvements in gain bandwidth product of parametric amplifiers by the use of a second pump. The purpose of this communication is to report on several important measurements made at AIL that were neglected by the author in the above referenced letter. Measurements made at AIL on a double pumped parametric amplifier indicate that 1) the sensitivity (not the broad-band noise factor) is degraded, 2) the amplifier generates a multitude of spurious outputs, and 3) the increase in gain-bandwidth is not real, but is only an apparent one dependent on method of measurement.

The parametric amplifier that was employed in our experiments used a MA 4254 varactor having a zero bias capacitance of 0.8 pf and operated at a signal frequency of 1800 Mc. The amplifier (with single pump-

[6] Received July 16, 1962.

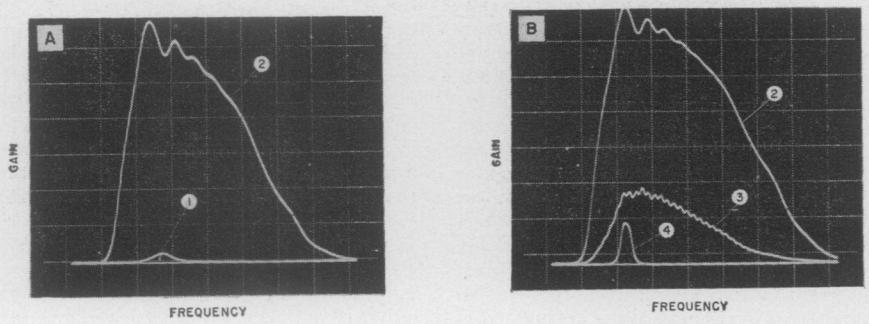

① SINGLE-PUMPED CASE
GAIN = 15 DB
② DOUBLE-PUMPED CASE
GAIN = 30 DB
PUMP FREQUENCIES = 10.150 AND 10.160 GC
③ OUTPUT RESPONSE WITH A DOUBLE-TUNED 10-MC PRESELECTOR ON THE OUTPUT TO THE DETECTOR
④ RESPONSE OF THE PRESELECTOR ALONE

Fig 1—Gain as a function of frequency.

TABLE I

	Signal Frequency	Gain	Measured Broad-band Noise Factor	MDS*
Single pump	1800 Mc	15 db	2.2 db	−108.8 dbm
Double pump	1800 Mc	16.5	2.0	−102.8
Double pump	1800 Mc	22.0	1.9	− 85.8

* MDS (minimum discernible signal) was measured with a 2.0 Mc post receiver bandwidth

ing) yielded a gain of 15 db with a 3 db bandwidth of 50 Mc. The measured over-all noise factor was about 2.2 db (with a second-stage noise factor of 11 db). Fig. 1A shows the measured performance of the amplifier with single pumping and double pumping (with a 10-Mc spacing between pumps). This measurement was made by use of a swept signal generator and a broad-band detector feeding a HP 130B scope. It was initially thought that the pump frequencies were leaking into the output detector producing unwanted responses, consequently, a low-pass filter having a cutoff frequency of 4000 Mc was added to the output (before the detector) and there was no significant change in the response.

A double-tuned 10-Mc wide band-pass filter was then inserted before the detector and the results are shown in Fig. 1B. The filter led to a decrease in apparent gain of the double-pumped parametric amplifier (shown in the middle curve), but it did *not* narrow the pass band as should obviously have occurred. The filter characteristic is also shown in Fig. 1B. The horizontal sweep corresponds to a frequency of 1.55 Gc at the low end and 1.9 Gc at the high end.

A noise factor measurement of the double-pumped parametric amplifier was made utilizing a helix noise generator, a double-tuned 10-Mc wide preselector and a mixer followed by a 30-Mc preamplifier and post amplifier combination. It was found that careful adjustment of the local oscillator had to be made to avoid regions of high spurious output. Discrete points of high noise spikes were found to exist approximately every 10 Mc (the double-pump spacing) as the local oscillator and preselector were varied. Table I lists the measured results obtained with a single-pumped and double-pumped parametric amplifier. Although the broad-band noise factor was relatively good, the CW sensitivity (MDS) was severely degraded.

We have not had the opportunity yet of making any theoretical investigations of the double-pumped case; therefore, we can base our conclusions only on the experimental evidence that we have obtained.

We believe the reasons for the discrepancies are:

1) The beating of the two pump oscillators results in a forced on-off modulation of the gain (if we assume equal pump voltages applied to the varactor) at a rate equal to the difference frequency (or beat rate) at the double-pump spacing. When the pump frequencies are in phase, we get reinforcement of the voltage and an attendant high gain condition, and when the pump frequencies are out of phase we get cancellation of the pump voltage and a corresponding low gain condition. This modulation will take place at the difference frequency (the difference between the two pump frequencies).

2) Spurious outputs are generated when a fixed input frequency is applied to the varactor. These outputs will be present over the entire bandwidth of the input circuit and will be separated in frequency by the difference in pump frequencies. This conclusion would explain why a narrow-band filter inserted in the output does not narrow the over-all pass band. The presence of spurious outputs also explains the discrepancy between the broad-band noise factor and the CW sensitivity.

3) Spurious outputs are present (of low amplitude) when no input signal is present. These outputs are separated in frequency by the difference between the pump frequencies. Consequently, the CW sensitivity is determined partly by the proximity to one of the spurious outputs.

The double-pumping scheme has been shown to be of questionable value as a means for obtaining a low-noise broad-band parametric amplifier.

T. N. DeFilippis
D. Neuf
P. Lombardo
Airborne Instruments Lab.
Deer Park, N. Y.

Author's Comment[7]

I am surprised that Messrs. DeFilippis, Neuf, and Lombardo, whom I respect for their work in parametric amplifier field, care to make far reaching conclusions about a device the amplification mechanism of which they admittedly do not understand.

I do not doubt the correctness of their measurements; it is a matter of fact that this is exactly what they had to expect if they understood the double-pumped parametric amplifier (DPPA). However, their general conclusions about the MDS and what they call "apparent bandwidth" are incorrect.

It is true that the MDS or radar noise figure (not radiometric noise figure) of a DPPA is worse than the MDS of the same amplifier driven by only one pump. However, this is true if, and only if, the bandwidth of the second stage amplifier (*i.e.*, the bandwidth of the 30-Mc IF amplifier used by DeFilippis, *et al.*) is narrower than the bandwidth of the DPPA.

The reason for this is that a DPPA not only amplifies a given CW input signal, but also converts it in 2 or more frequencies spaced by $\Delta\omega$, the pump frequencies difference, on either side of the original signal frequency. (All these frequencies are within the signal bandwidth of the amplifier.) There are therefore 3 different gains of a DPPA:

1) Straight amplifier gain, that is,
(power out at the signal frequency)/(max. available power in at the signal frequency).
This gain is the dominant one.
2) Converter gain, that is,
(power out at a frequency different by $\Delta\omega$ from the original signal frequency)/(max. available power in at the signal frequency).
The converter gain is about 6 db below the straight amplifier gain.
3) Total gain, that is,
(total power out at all frequencies within the signal tank bandwidth)/(max. available power in at the signal frequency).

The 3 gains are shown in Fig. 2 and Fig. 3, which are computed responses of a DPPA with two different values of the pump spacing factor "n" (defined in Fig. 2). The sig-

[7] Received September 4, 1962.

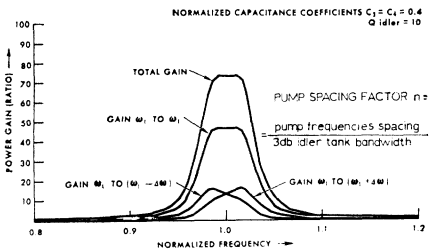

Fig. 2—Computer plot of gain vs frequency response of the double-pumped parametric amplifier. Pump spacing factor $n=0.45$.

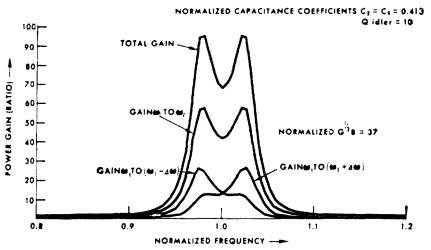

Fig. 3—Computer plot of gain vs frequency response of the double-pumped parametric amplifier. Pump spacing factor $n=0.5$.

nal tank bandwidth is assumed to be 3 times the pump frequencies spacing $\Delta\omega$. The formidable equations used to compute the gain curves can not be shown here because of lack of space. I have to refer to the publication of the complete theory of the DPPA, mentioned in my original correspondence.[1]

If a DPPA is connected in front of a second stage amplifier, the bandwidth of which is narrower than the pump frequency spacing $\Delta\omega$, then a coherent signal at a frequency say 1 in Fig. 2 will be amplified such that the majority of the output power will be at the original signal frequency (gain ω_1 to ω_1), but some portion of the output power will be lost, because the second-stage amplifier is too narrow to utilize gains ω_1 to $(\omega_1 \pm \Delta\omega)$. Therefore the coherent signal gain will be, for example in Fig. 2, equal to 45.

However, a noise signal entering the amplifier will be straight amplified *and* converter amplified, because input noise power contained in a bandwidth equal to the IF-amplifier bandwidth and centered at 1 will be amplified 45 times (in Fig. 2), but in addition to it two input noise bands of the same bandwidth as the IF amplifier and centered at frequencies $(\omega_1 - \Delta\omega)$ and $(\omega_1 + \Delta\omega)$ will be amplified about 15 times and converted to a noise band centered at the original signal frequency. Therefore, if no excess noise is generated by the DPPA, the output SNR for coherent signals will be by a factor of 75/45 worse than the input SNR in this specific case.

This output SNR degradation will be even more severe if the pump spacing factor "n" is much smaller than in the above cases or if the gain of the amplifier is increased. This is so because with larger pump drive additional sidebands will be generated (that is $\omega_1 \pm 2\Delta\omega$, $\omega_1 \pm 3\Delta\omega$, etc.), thus folding more and more output noise power into the original signal band; this explains the MDS degradation with larger gain, as observed by DeFilippis, *et al.* Obviously, the MDS degradation will be much smaller, if any, if the antenna temperature of the receiver is low and the pump spacing factor is at least 0.5.

The MDS degradation can be eliminated completely, regardless of the antenna temperature, amplifier gain and pump spacing if the second stage amplifier has the same bandwidth as the DPPA. In this case the total gain for coherent and noise signals is effective, resulting in equal radar and radiometric noise figures. Because the excess noise temperature of a DPPA is always smaller than the excess noise temperature of a SPPA with equal bandwidth (for proof see the theoretical paper[1]), the MDS of a DPPA will actually be smaller.

It should be pointed out that such a comparison can not be made by simply adding a pump to an existing SPPA. Such a comparison is incorrect not only because the bandwidth of the double-pumped amplifier is always bigger than the bandwidth of the same amplifier driven by only one pump (in spite of a narrow band-pass filter connected to the *output* of the par. amplifier), but also because the optimum design parameters of the DPPA, such as input impedance, f_i to f_s ratio and effective filling ratio are not equal to the design parameters of an SPPA.

Because for CW signals the total output power of a DPPA is distributed among many frequencies separated by $\Delta\omega$, the amplifier can not be used for applications at which the carrier is modulated with frequencies higher than $\frac{1}{2}\Delta\omega$. However, in a practical case the pump frequency difference $\Delta\omega$ should be in the order of perhaps 500 Mc such that this application limitation of the DPPA is not very serious.

I believe that it should be obvious why DeFilippis, *et al.*, measured less gain but essentially the same bandwidth even after a 10-Mc wide bandfilter was inserted between the par. amplifier and detector. They simply measured either the converter gain or the straight amplifier gain, depending on the instantaneous frequency, but not the total gain as they did before the insertion of the bandfilter. Since all the gains have essentially the same bandwidth, no bandwidth reduction could have been observed.

The high "noise" spikes observed by DeFilippis, *et al.*, are actually gain peaks and they occur only if the pump spacing factor is large and the amplifier is pumped hard. This can be observed by comparing Fig. 2 and Fig. 3. In Fig. 3 two gain spikes are visible, while no spikes exist in Fig. 2. The gain spikes can be made up to 100 times larger than those in Fig. 3 by merely increasing the coefficients C_3 and C_4 (*i.e.*, pump drive). That the "noise" spikes are actually gain spikes was determined experimentally by measuring the radiometric noise figure in the region of the spikes. The over-all receiver noise figure was minimum at these frequencies, proving that the noise spikes are highly amplified input, not excess noise of the DPPA.

In contrast to the "noise" spikes the spurious outputs of low amplitude observed by my critics in the absence of CW input signal are separated exactly by the pump spacing $\Delta\omega$. They are the harmonics of the $\Delta\omega$ frequency (in the AIL case they were the 180th, 181st, etc. harmonics). They can be eliminated by terminating the $\Delta\omega$ frequency reactively, which is important also for other reasons.

I am puzzled by the statement of my critics that the increase in gain-bandwidth is only apparent. I believe that their statement is based on the erroneous assumption that the DPPA is something like an SPPA, the gain of which is "chopped" at the $\Delta\omega$ frequency. In this case a wide bandwidth illusion could be generated in that a narrow input band would be "folded out" in a wide output band. This is not the case, however. The DPPA is electrically equivalent to a number of staggered tuned parametric amplifiers, where each of the hypothetical amplifiers has the same idler frequency but different pump frequency, thus providing gain for a number of adjacent signal bands.

It was shown that the conclusions of Messrs. DeFilippis, Neuf, and Lombardo, based on a superficial investigation and the lack of understanding of the DPPA, are incorrect.

Double pumping is the only broad-banding concept known to me which results in a very substantial bandwidth increase of parametric amplifiers without any degradation of broad-band noise figure and, when properly used, without any degradation of radar noise figure as well. With the exception of broad-band frequency multiplex systems it is vastly superior to any other par. amplifier configuration not only for radiometric applications, for which it was originally conceived, but also for systems applications in which a wide instantaneous bandwidth and maximum sensitivity for CW signals is required. Its value is in my opinion not more questionable than the value of a single-pumped broadband par. amplifier, the bandwidth of which depends on the availability of highly selected varactors or even pairs of such varactors.

GEORGE C. SPACEK
P.O. Box 3671
Santa Barbara, Calif.

Optical Mixing in Phototubes*

The photo emission phenomenon as a tool for optical mixing was first investigated by Forrester, *et al.*[1] Siegman and McMurtry[2] have demonstrated the use of a traveling-wave tube with a photocathode as a tool for observing the optical mixing of various axial modes of a ruby laser and have suggested the use of such TWT's as detectors of microwave modulated laser beams. In addition, several other schemes of light

* Received September 12, 1962.

[1] A. T. Forrester, R. A. Gudmundsen, and P. O. Johnson, "Photo-electric mixing of incoherent light," *Phys. Rev.*, vol. 99, pp. 1691–1700; September 15, 1955.
[2] A. E. Siegman and B. J. McMurtry, "Photomixing experiments with a ruby optical maser and a traveling-wave microwave phototube," *Appl. Optics*, vol. 1, pp. 51–53; January, 1952.

demodulation using semiconductor diodes[3,4] and photomultipliers[5] have been proposed and demonstrated. The purpose of this communication is to describe photomixing experiments in which a specially constructed microwave tube has been replaced by a low-cost device utilizing a commercially available phototube as an efficient light demodulator operating at microwave frequencies.

The phototube used in our experiments was a miniature RCA 1P42, inserted in a holder designed to match the phototube output to either a 50-ohm coaxial line or a waveguide. Figs. 1 and 2 show the design of the coaxial and waveguide holders. The block diagram of the experimental setup is shown in Fig. 3. The microwave output from the phototube was fed into a low-level S-band TWT and then, after amplification, to a crystal detector.

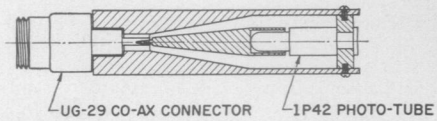

Fig. 1—Structure of coaxial phototube holder.

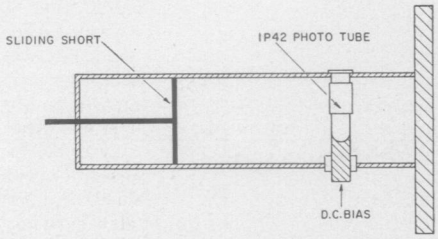

Fig. 2—Structure of waveguide phototube holder.

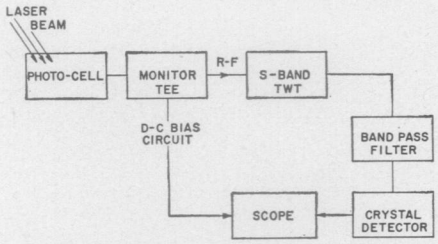

Fig. 3—Block diagram of the experimental setup.

An elliptical cavity laser with a $2\frac{1}{2}$ inch ruby rod was used as a light source in our experiments. For this ruby length, the axial modes are separated by approximately 1.3 kMc, so that the difference frequencies of modes separated by 2 and 3 intervals can be observed in the S-band setup: The two sets of difference frequencies at 2.6 and 3.9 kMc have been experimentally identified with help of a band-pass filter inserted between the amplifier and the crystal. A set of typical results from the phototube in the coaxial holder is given in Fig. 4. Similar results were obtained using the waveguide holder. The output amplitudes obtained with the phototube detector are of the same order of magnitude as those we measured previously in performing the same experiment with a specially constructed photo-TWT (Sylvania SY4302) used as a detector.

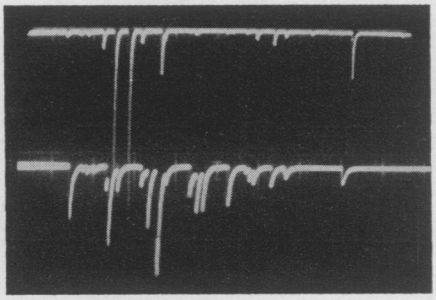

Fig. 4—Microwave components as detected and displayed on oscilloscope. In order to confirm the presence of both difference frequencies, the output of the TWT amplifier has been divided by use of high-pass and low-pass filters into the 3.9 kMc component (upper trace) and the 2.6 kMc component (lower trace). Amplitude scale is 20 mv/div upper trace and 200 mv/div lower trace. Time scale is 50 μsec/div.

The phototube detector, like the *PIN* diode detector,[3] is inherently limited in high-frequency response by the transit time involved. For the RCA 1P42, the transit time is calculated to be approximately 3×10^{-10} sec. By reducing the cathode-anode separation and increasing the bias voltage, one can expect to improve the high-frequency response. The sensitivity could also be improved by using a photocathode surface with better response characteristics in the laser frequency region. The RCA 1P42 cathode has the S-9 surface which has a very weak response to the laser frequency. An S-1 surface should give much greater sensitivity. Using a nonminiaturized phototube with the S-1 response (RCA 925) and a very crude microwave circuitry, we have been able to obtain results similar to the ones shown in Fig. 4. The larger cathode-anode separation and the poor RF match in the RCA 925 tube are partially compensated for by higher bias voltage and more favorable photosurface response characteristics.

We conclude that an ordinary phototube may be used as an efficient low-cost optical mixer and light demodulator. With tubes currently available in the market, the beat frequencies up to S band can be detected with this type of device. By properly designing the tube for this particular application, it should be possible to fabricate phototubes capable of detecting much higher beat frequencies.

P. A. Lindsay
S. F. Paik
K. D. Gilbert
S. A. Rooney
Research Div.
Raytheon Co.
Burlington, Mass.

[3] H. Inaba and A. E. Siegman, "Microwave photomixing of optical maser outputs with a *PIN*-junction photo-diode," Proc. IRE (*Correspondence*), vol. 50, pp. 1823–1824; August, 1962.
[4] L. U. Kibler, "A high-speed point contact photodiode," Proc. IRE (*Correspondence*), vol. 50, pp. 1834–1835; August, 1962.
[5] O. L. Gaddy and D. F. Holshouser, "Photomultiplier detection of microwave modulated light," Proc. IRE (*Correspondence*), vol. 50, p. 1525; June, 1962.

Light Triggered Oil Waves*

In a recent program at the General Electric Electronics Laboratory, Syracuse, N. Y., a two dimensional light amplifier has been constructed from successive uniform layers of a conductor, a photoconductor and an insulating oil. When such a sandwich is uniformly charged with an ion charging technique, it acts as a sensitized photographic plate. Both the photoconductor and oil are insulators in the dark and the applied voltage is distributed in accordance with their respective dielectric constants and thickness. Exposure of the photoconductor, to an image, shorts its portion of the series capacitance arrangement. Whenever exposed areas are in close proximity, strong local fields are created which cause the oil to flow in response to the applied forces.

After these oil waves have developed, the exposed picture can be projected for viewing by the reflective Schlieren optics. The fact that the oil waves, once created, are not destroyed by the viewing light is a result of the fact that the entire area is flooded with light often much more intense than the exposing light. This uniform illumination does not create any local forces that will alter the wave system. Of course, surface-tension forces eventually remove the wave image.

All of the work so far has used amorphous selenium as the photoconductor. The selenium has a black to reddish color but can be obtained with a mirror-like surface which will reflect from 35–50 per cent of the incident light. The transparent oil, when applied to its surface, does not materially affect this property. This mirror property is particularly important to the image projection process.

Oil thickness and the wave development time are important process parameters in addition to those relating to photographic exposure and sensitivity. To evaluate the effect of these parameters, an experimental equipment was constructed which is shown symbolically in Fig. 1. The oil is applied to the selenium covered aluminum electrode by a wiper and then charged by an ion charging grid. The exposing and viewing operations, shown separately for convenience, were combined to avoid the necessity of mechanical indexing. Xenon flash lamps and time delay circuits were used to determine the process development time. Because of the instantaneous nature of the flashed viewing lamp, this light was used to obtain photographic recordings of the oil film deformation.

While an accurate measurement of the oil wave amplitude has not been made, an estimate of the amplitude delay-time characteristic has been obtained. It has been found that when the oil thickness was about 5 per cent of the spatial wavelength, a maximum response was achieved. This spatial wavelength is controlled by a photographic ruling which is imaged by the exposure lens. Therefore, both thickness and spatial wavelength are important process parameters. While the best pictures have

* Received September 17, 1962.

been obtained for spatial wavelengths between 120 and 60 microns, 8 to 16 lines/mm, some pictures have been obtained for frequencies as high as 35 lines/mm. A considerable range in the development time has been encountered. Good pictures are obtainable for as short a time as 1 msec, or as long as a minute depending on both the oil viscosity and film thickness.

Because the active surface, the selenium oil interface, is below the oil air surface, the penetration of the voltage variation of this active surface through the oil to the deformable oil air surface is related to the ratio of oil thickness to spatial wavelength. Such a problem is not encountered when a charge variation is applied to the oil-air surface. Because of difficulties in controlling

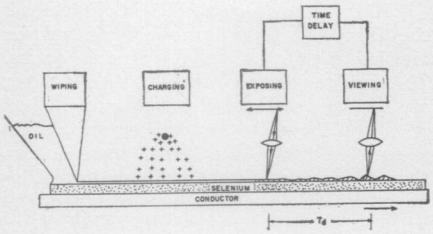

Fig. 1—Schematic of the light triggered oil film technique.

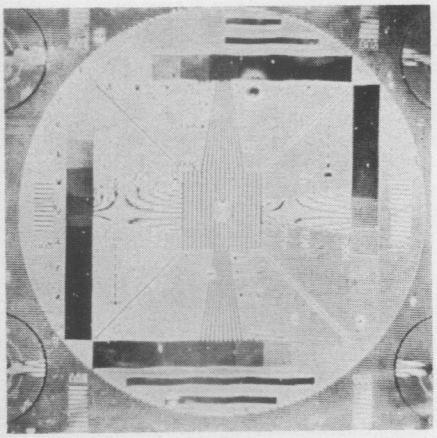

Fig. 2—Oil film surface deformation in response to an RTMA test chart input.

the oil films, a practical device would probably use a 60-micron wavelength requiring, therefore, an area roughly $1\frac{1}{4}$ by $1\frac{1}{2}$ inches for a standard TV picture. It should also be noted that the 1-msec development time and 16-msec viewing time necessary for TV projection are readily obtainable. Proper exposure of the selenium with light from a cathode-ray tube has been described in numerous articles and has been successfully employed to produce in-air oil film deformation. Both grey scale and resolution capability are indicated in Fig. 2 which is a photograph of the oil film surface deformation in response to an RTMA test chart input.

R. B. GETHMANN
Electronics Lab.
General Electric Co.
Electronics Park
Syracuse, N. Y.

Performance of a Regenerative Limiter in FM Receivers*

It has recently been suggested by Baghdady[1,2] that, by applying strong regenerative feedback around the limiter, a substantial reduction of the threshold carrier-to-noise ratio of FM receivers can be obtained. However, it can be shown that the output SNR of such a limiter does not significantly exceed that of an ordinary limiter under conditions representative of conventional receiver design practice. The promise for a real suppression of the FM noise threshold by a regenerative limiter thus appears open to debate.

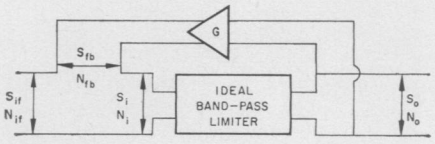

Fig. 1—Regenerative limiter—block diagram.

From consideration of Fig. 1, the following equation can be written

$$\frac{\sqrt{S_0/N_0}}{\sqrt{S_{if}/N_{if}}} = -R_N\sqrt{S_{fb}/S_{if}} + \sqrt{(R_N^2+\gamma-1)(S_{fb}/S_{if})+\gamma(1+2R_S\sqrt{S_{fb}/S_{if}})} \quad (1)$$

where the S and N represent signal and noise power, respectively, the R's are feedback-IF correlation coefficients, and γ is defined by $(S_0/N_0)=\gamma(S_i/N_i)$. This relation is also given by Baghdady,[1,2] with the signal correlation $R_S=1$. Neglecting loop phase shift, the noise correlation for respectively strong- and vanishing-signal conditions is $R_N=\frac{1}{2}\sqrt{2}$; $R_N=\frac{1}{2}\sqrt{\pi}$. We need here only note that axiomatically $R_S\leq 1$.

The quantity γ has been calculated by Davenport[3] and independently by Blachman[4] for Gaussian noise at the limiter input. Here, however, most of the limiter input noise is fed back from the output, and because the limiter drastically alters the noise statistics the same values for γ cannot be expected to hold. In fact for strong regenerative feedback, *i.e.*, $S_{fb}/S_{if}\gg 1$, practically all of both the signal and noise present at the limiter input are linearly amplified replicas of the corresponding outputs. Therefore a value of γ close to unity must characterize a strongly regenerative limiter, quite independently of S_{if}/N_{if}.

With the compatibility of the relationships $\gamma\cong 1$ and $S_{fb}/S_{if}\to\infty$ so established, the first can be used to simplify (1) and the second to show the ultimate effect of strong regenerative feedback on the limiter SNR's. Thus (1) yields

$$\lim_{(S_{fb}/S_{if})\to\infty}\left[\frac{\sqrt{S_0/N_0}}{\sqrt{S_{if}/N_{if}}}\right] = \frac{R_S}{R_N} \leq \frac{1}{R_N}. \quad (2)$$

It is apparent from (2) that the correlation coefficient of feedback and IF noise is a leading determinant of regenerative limiter performance, and that the meaning of results obtained by completely neglecting R_N is somewhat unclear. Actually, substitution of the foregoing values for R_N into (2) shows that the application of arbitrarily strong regenerative feedback around the limiter does not greatly alter well-known SNR relationships, and hence that little if any suppression of the FM receiver noise threshold can be predicted. Baghdady concurs[5] in this observation of the importance of R_N; the result is obvious upon reflection that we have actually treated the application of memoryless feedback around the limiter, which cannot affect the zero-axis crossings of the sum of IF signal and noise, and therefore can scarcely alter FM receiver performance.

The kernel of the problem then is to establish quantitatively the permissibility of feedback memory, *i.e.*, phase shift, and determine its effect on the correlation coefficient R_N. From the limiter-input signal voltage phasor diagram of Fig. 2, it is evi-

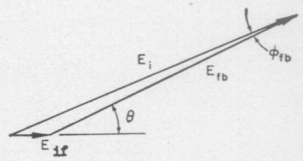

Fig. 2—Limiter-input phasor diagram.

dent that the closed loop feedback-IF phase shift is the angle θ. Further, since $E_{fb}=GE_0$ (where G is a real number), then for distortionless FM transmission, θ must be a linear function of signal frequency deviation. This can be satisfied if the open loop phase shift ϕ_{fb} (due to frequency-selective coupling networks) is a linear function of frequency deviation, and θ is permitted to be no greater than about $\frac{1}{2}$ radian over the entire range of signal-frequency deviation. However, the IF noise bandwidth and the range of signal-frequency deviation normally are quite comparable; the signal-linearity condition on θ then allows relating the simple concept of closed loop group delay $T=d\theta/d\omega$ to the effect of permissible feedback memory on the noise correlation coefficient $R_N(T)$.

* Received November 3, 1961; revised manuscript received July 23, 1962.

[1] E. J. Baghdady, "Lectures on Communication System Theory," McGraw-Hill Book Co., Inc., New York, N. Y., pp. 540–546; 1961.

[2] E. J. Baghdady, "A technique for lowering the noise threshold of conventional frequency, phase and envelope demodulators," IRE TRANS. ON COMMUNICATIONS SYSTEMS, vol. CS-9, pp. 194–206; September, 1961.

[3] W. B. Davenport, Jr., "Signal-to-noise ratios in band-pass limiters," *J. Appl. Phys.*, vol. 24, pp. 720–727; June, 1953.

[4] N. M. Blachman, "The output signal-to-noise ratio of a power-law device," *J. Appl. Phys.*, vol. 24, pp. 783–785; June, 1953.

[5] Baghdady, *op. cit.*, p. 202.

Specifically, we are concerned with the behavior of the envelope of this quantity $\hat{R}_N(T)$, since the higher "frequency" variations of both $R_S(T)$ and $R_N(T)$ are related to the IF carrier in the same way. Using the results of Bussgang,[6] which show that the cross correlation between the input and output of the limiter is proportional to the autocorrelation function of the input, it follows that $\hat{R}_N(T)=\frac{1}{2}\sqrt{\pi}\hat{R}_{if}(T)$, where $R_{if}(T)$ refers to the autocorrelation coefficient of the IF noise. Assuming $|\theta|=\frac{1}{2}$ at the edges of a rectangular IF pass band B cps wide, then $T=1/2\pi B$, and introducing $R_{if}(T)=(\sin \pi BT)/\pi BT$, we find that $\hat{R}_N(1/2\pi B)=0.85$; not much less than $R_N(0)=\frac{1}{2}\sqrt{\pi}=0.885$, as concerns the vanishing-signal performance indicated by (2). Thus, even with the maximum permissible feedback memory, about 0.4 db is the maximum extent to which a regenerative limiter can be expected to improve FM receiver performance: "maximum" in that we have neglected the fact $\hat{R}_S(T)<R_S(0)$ for a modulated carrier.

It is the conclusion of this note that a regenerative limiter is not capable of significantly improving the random-noise threshold performance of an FM receiver, under customary design constraints and practices. An exception to this can be visualized only in the uncommon situation where the IF noise bandwidth greatly exceeds the total range of signal-frequency deviation to be accommodated.

J. J. Downing
Commun. Res., Lockheed Missiles and Space Co.,
Palo Alto, Calif.

[6] J. J. Bussgang, "Cross-correlation functions of amplitude-distorted Gaussian signals," Mass. Inst. Tech., Cambridge, Mass., RLE TR no. 216, pp. 4–13; March, 1952.

Author's Comment[7]

Downing has drawn a very sweeping conclusion from an argument of very restricted validity. Missing in this argument is a more accurate reference to what I have actually "suggested," and a greater awareness of the significance of certain results and the conditions under which they hold.

What I have shown[1,2] (and which has also been amply demonstrated experimentally) is that "a substantial reduction of the threshold carrier-to-noise ratio of FM receivers can be obtained" with an *oscillating limiter* whose oscillation is sufficiently strong to bring about the minimum acceptable degree of noise quieting when only the noise and no signal is present. The key assertion in my argument[1,2] is that if the level of the oscillation compared to the level of the ambient random-fluctuation noise is sufficient to quiet the noise, then a signal that is capable of suppressing the oscillation *in the absence* of the input noise over some range of instantaneous frequency values should also be able to overpower the oscillation *in the presence* of the noise and appear dominant over the noise in the output. Since the signal amplitude that is necessary to overpower the oscillation depends directly upon the product of oscillation amplitude at the input of the limiter and the open-loop (nonzero) delay, the value of this product must be adjusted to the minimum possible that will ensure the desired degree of quieting and will allow signal "lock" over the desired range. This will reduce to a minimum the threshold that the signal must exceed in order to overpower the oscillation, and this threshold will fall below the threshold of a conventional demodulator.

In Downing's discussion, (1) holds subject to the conditions that a feedback steady state exists in which only the signal and the noise are present and the oscillation (if it existed before the introduction of the signal) has been suppressed by the signal or the noise. Only the condition in which the introduction of the signal suppresses the oscillation is of interest, because it can be shown that no improvement can result if the noise in the absence of signal prevents a coherent oscillation from being established (or operationally, if no significant noise squelch or quieting can be observed when the regenerative feedback is introduced). Completely oblivious of all the conditions that must be satisfied, Downing manipulates (1) toward a limiting value at which it would hold only if a locking range of zero width is acceptable and hence only a signal of zero bandwidth (*i.e.*, a pure unmodulated carrier) can be passed through the closed-loop system. If $(S_{fb}/S_{if})\rightarrow\infty$, then either the signal frequency must coincide with the frequency of zero feedback phaseshift in order to be passed by the system without violent distortion or $\phi_{fb}(\omega)\equiv 0$ must hold over the entire range of signal frequency excursions. In the former case the degree of improvement depends upon the degree of coherence of the oscillating limiter output in the presence of the pure noise input; in the latter case I have shown[2] that a degradation of SNR results for low values of $(S/N)_{if}$ and an improvement by a factor of 2 occurs for high values of $(S/N)_{if}$.

Downing's (2) is, therefore, of no value as a basis for evaluating the effect of regenerative feedback upon SNR under arbitrary conditions. It applies only under conditions of "memoryless feedback" as long as the amount of feedback far exceeds the IF noise.

Downing's evaluation of the correlation coefficient between noise fed back and IF noise is not valid under the conditions postulated. It ignores completely, and thus assumes away, the very basis for the S/N improvement necessary for threshold reduction. Under the conditions postulated by Downing, the fundamentals of feedback theory demand that the system oscillate strongly at the frequency of in-phase feedback. With a strong oscillation present, the noise bandwidth as observed at the limiter output will be narrower than the noise bandwidth in the absence of feedback by a factor of $\beta(\gg 1)$, say. This noise bandwidth reduction factor within the loop is a measure of the degree of "coherence" of the self-sustained oscillation in the presence of the input noise. The higher the value of β, the "cleaner" the oscillation as seen at the limiter output will be. These effects can be demonstrated on an oscilloscope screen in the laboratory. Reduction of the bandwidth of the noise fed back by a factor of β reduces the correlation coefficient between IF noise and noise fed back by a factor of $\sqrt{\beta}$.

Additional insight into oscillating limiter operation can be gained from the treatment of the dynamics of a signal-squelched oscillating limiter to be presented by this writer.[8]

Elie J. Baghdady
ADCOM, Inc.
Cambridge, Mass.

[8] E. J. Baghdady, "Dynamics of a signal-squelched oscillating limiter with app ication to noise threshold reduction," submitted for the Correspondence Section of Proc. IRE.

[7] Received September 11, 1962.

Correction to "A Technique for Equalizing Parabolic Group Delay"*

In the above correspondence[1] the author would like to make the following corrections:

Eq. (1) should read

$$\theta = -\sum_{b=1}^{n} \tan^{-1}\frac{X - X_{bi}}{X_{br}}.$$

Line five should read "X_{br} and X_{bi} are real and imaginary · · · ."

Eq. (13) should read

$$d = \frac{1}{\pi\Delta f}\sum_{r=1}^{n}\frac{B_r}{1+(A_r+B_{rX})^2}.$$

Eq. (14) should read

$$d_0 = \frac{1}{\pi\Delta f}\sum_{r=1}^{n}\frac{B_r}{1+A_r^2} = \frac{D_0}{\pi\Delta f}.$$

R. M. Kurzrok
RCA Surface Commun. Sys. Lab.
New York, N. Y.

* Received August 8, 1962.
[1] R. M. Kurzrok, Proc. IRE (*Correspondence*) vol. 50, p. 1840; August, 1962.